



Interatomic potentials for oxide glasses: Past, present, and future



Alfonso Pedone ^{*}, Marco Bertani, Luca Brugnoli, Annalisa Pallini

Department of Chemical and Geological Sciences, University of Modena and Reggio Emilia, via G. Campi 103, 41125 Modena, Italy

ARTICLE INFO

Keywords:

Molecular dynamics simulations
Interatomic potentials
Oxide glasses
Structure
Properties

ABSTRACT

The continuous development and improvement of interatomic potential models for oxide glasses have made classical molecular dynamics a powerful computational technique routinely used for studying the structure and properties of such materials on a par with the more advanced experimental techniques.

In this brief review, we retrace the development of the most used interatomic potential models from the earliest MD simulations up to now with a look at the possible future developments in this field due to the advent of the machine learning era and data-driven methods.

1. Introduction

Since its first application to the investigation of the structure of vitreous silica in 1976, [1] classical Molecular Dynamics Simulations have become an effective and indispensable technique to study the complex atomic structure and the structure-properties relationships in glassy materials. Despite significant progress witnessed in the last decades, the application of MD simulations to study glasses and in particular multicomponent systems still faces several challenges.

In this short review, we will focus on the most critical ingredient of classical MD simulations: that is the interatomic potentials. Firstly, the ability to perform MD simulations of a particular glass composition is limited by the availability of the interatomic potential parameters for the interacting elements in the system. Secondly, the accuracy and validity of the results are largely determined by the quality of the interatomic potential model used and its parameterization.

An alternative approach to overcome these limitations would be to resort to *ab initio* MD simulations in which the forces are obtained from accurate first principle calculations. [2] If the first principle theory used can adequately describe the chemical bonding in the system this approach is more general and can be applied to any glass system. However, the price to pay is the extremely high computational cost, which limits its applicability to relatively small systems (up to a few hundreds of atoms) for a short timescale (tens of picoseconds). For these reasons, this technique is mainly used to study the short-range structure and vibrational dynamics of systems for which reliable force fields have not been developed yet or when a higher accuracy must be reached.

In the following sections, we will concentrate on the empirical force

fields mostly used in the past, nowadays, and on the models that will be probably developed in the future. The discussion will be limited to the interatomic potential models for multicomponent oxide glasses.

2. A historical overview of interatomic potentials models

In atomistic computer simulations, the total potential energy (U) of a system containing N atoms is generally broken down into various terms, such as individual (U_i), pair (U_{ij}), three-body (U_{ijk}), and higher-order terms depending on the chemical-physical features of the system under study.

$$U = \sum_i U_i + \sum_i \sum_{j>i} U_{ij} + \sum_i \sum_{j>i} \sum_{k>j} U_{ijk} + \dots \quad (1)$$

The first term represents the effect of an external field on the i^{th} atom. The second term represents the potential between the i^{th} and j^{th} atoms and the third term represents three-body interactions between three atoms.

In the past 40 years, a multitude of interatomic potential models has been developed and applied to study the structure and properties of oxide glasses. In the following, the different force fields have been grouped based on three major models: i) the rigid ionic models; ii) polarizable models and iii) reactive force fields.

2.1. The rigid ionic models

In the early investigations carried out between 1976 and 1985, [1,3–9] it was common to approximate the total energy by using only

* Corresponding author.

E-mail address: alfonso.pedone@unimore.it (A. Pedone).

two-component terms based on the Born-Mayer-Huggins (BMH) potentials composed of a long-range Coulomb term and a short-range term to mimic the repulsion between electron charge clouds:

$$U_{ij}(r) = \frac{q_i q_j e^2}{r} + \left(1 + \frac{q_i}{n_i} + \frac{q_j}{n_j}\right) b_{ij} e^{[(\sigma_i + \sigma_j - r)/\rho_{ij}]} \quad (2)$$

In this expression, q is the charge on atoms i and j , e is the proton charge, n is the number of outer shell electrons, σ is a distance parameter characteristic of the ionic radius, and b and ρ are constants. In some cases, a modified BMH potential in which the Coulomb term is attenuated by an $erfc$ function and the second short-range term is replaced by a term of the type $A_{ij}e^{-r/\rho_{ij}}$ could be found.

By using a functional form of this type, full formal charges (Si^{4+} , O^{2-} ...) on the constituting ions but different potential parameters, Woodcock et al. [1] were the first to simulate the vitreous transition and structure of pure silica; Soules [3–5] simulated the structure of some sodium silicate, soda-lime glass, sodium borosilicate, sodium-potassium, and aluminosilicate glasses whereas Garofalini et al. [8,9] investigated the bulk and surface structure of vitreous silica and alkali silicate glasses.

These simulations produced random network silicate structures as proposed by Zachariasen. [10] The sodium ions create non-bridging oxygens (NBOs) and occupy interstitial sites with a not well-defined coordination environment. Ribbons and sheets of regular BO_3 triangles linked through apices made up the structure of vitreous B_2O_3 . In borosilicate glasses, the conversion of BO_3 to BO_4 units was observed with the addition of sodium ions whereas in sodium aluminosilicate glasses aluminum was always found to prefer four-fold coordination. [3]

Despite the interesting results of these pioneering and fundamental works, the comparison with experimental measurements (X-ray and Neutron diffraction, RAMAN, and NMR spectroscopy), the high amount of over-coordinated silicon ions, and the irregular tetrahedral geometry of the SiO_4 units found in MD-derived structures revealed that the covalent nature of the Si-O bond was too strong to be neglected. As for borates and borosilicate glasses, no boroxol rings (planar 6-membered rings of B and O) have been observed with pair-wise interatomic models [3,5,11,12] as instead identified by the extremely sharp line at 808 cm^{-1} in the Raman spectrum [13] and quantified by neutron diffraction [14] and NMR experiments. [15]

To the best of our knowledge, Feuston and Garofalini were the first to introduce three-body potentials for O-Si-O and Si-O-Si triplets of atoms to study pure silica and sodium trisilicate glasses in 1988. [16,17] Albeit, a few years before Sanders et al. [18] proposed the first shell-model potential with three-body terms for the O-Si-O angle it was applied to study α -quartz and other SiO_2 polymorphs. In the subsequent two years, Vessal et al. [19] and Vashishta et al. [20] also proposed their three-body potentials for silica glass. The functional forms were all different. In the following, we report only the so-called Vessal-Amini-Leslie-Catlow (VALC) potentials because this was extensively used, in conjunction with cations-oxygens pair potentials developed for oxides by Lewis and Catlow [21] and minerals by Parker et al. [22], to study multicomponent oxide glasses in the subsequent years by Huang and Cormack, [23–25] Smith, Greaves and coworkers. [26–28]

In the VALC model, the short-range interactions between different ions were modeled by a four-range Buckingham potential of the form:

$$U_{ij}(r) = A_{ij} e^{-\frac{r_{ij}}{\rho_{ij}}} r_{ij} < r_1$$

$$U_{ij}(r) = \sum_{m=0}^5 A_m r_{ij}^m r_1 < r_{ij} < r_2$$

$$U_{ij}(r) = \sum_{m=0}^3 B_m r_{ij}^m r_2 < r_{ij} < r_3$$

$$U_{ij}(r) = -\frac{C_{ij}}{r_{ij}^6} r_3 < r_{ij} < r_c \quad (3)$$

Where r_c is the short-range cutoff, A_{ij} , ρ_{ij} and C_{ij} are parameters that were determined by fitting to experimentally measured crystal structures and properties and the others are constants to be determined to spline the function at r_1 , r_2 , and r_3 making it continuous and derivable.

Two different forms for the three-body interactions have been used with the above two-body potential to describe the O-Si-O and Si-O-Si angles, respectively:

$$\begin{aligned} U_{ijk}(r_{ij}, r_{ik}, \theta_{ijk}) &= \frac{1}{4} A_{ijk} B_{ijk}^2 e^{-\frac{r_{ij}}{\rho_1}} e^{-\frac{r_{ik}}{\rho_2}} \\ A_{ijk} &= \frac{k_{ijk}}{2(\theta_0 - \pi)^2} \\ B_{ijk} &= (\theta_0 - \pi)^2 - (\theta_{ijk} - \pi)^2 \end{aligned} \quad (4)$$

$$U_{ijk}(\theta_{ijk}) = k_{ijk} \left[\delta_{ijk}^n (\delta_{ijk} - \theta_0)^2 (\theta_{ijk} - \theta_0 - 2\pi)^2 - \frac{n}{2} \pi^{n-1} (\delta_{ijk} - \theta_0)^2 (\pi - \theta_0)^3 \right] \quad (5)$$

With the adoption of the aforementioned potentials, the structures of silica glass and alkali silicate glasses obtained by MD simulations were in better agreement with experiments not only in terms of Si-O distances but also for the intra- and inter-tetrahedral angles. [16,19,20] Therefore, a great improvement was observed for the short range-order of oxide glasses. The investigations on binary alkali [23,24,26,27,29] and mixed alkaline silicate glasses [25,30,31] revealed a heterogeneous structure at the atomic level with the alkali-metal ions and non-bridging oxygens forming clusters and percolation channels within the silica matrix and thus corroborating the *modifier random network model* proposed by Greaves on the bases of EXAFS studies. [32,33]

Mixed alkali silicate glasses have been also studied in detail by molecular dynamics simulations to understand the microscopic origin of the mixed alkali effect (MAE) on ionic diffusivity. [31,34] In general, the observation was that albeit the different types of alkali-metal ions are rather randomly distributed with respect to one another within the alkali-metal-rich regions, their local structure (coordination environment) and site potentials are rather different. As a result, alkali ions preferentially jump only to like-ion sites and the MAE has been attributed to the blockage of preferred migration paths in mixed-alkali compositions (see Fig. 1). [35]

To better reproduce the B-O-B angle and hopefully also the formation of boroxol rings in borates and borosilicates glasses Hirao and Soga [36] applied an attractive potential with an exponential form to the B-B interactions whereas Inoue et al. [37] included a three-body interaction for O-B-O and B-O-B angles by putting a ghost atom with a positive point charge on the centroid of both the BO_2 and B_2O triangles. The latter observed boroxol rings, even if with a lower amount (22.5% of boron atoms were engaged in boroxol rings) with respect to experiments (that ranges between 60 and 80%). [14,15] Despite this quantitative disagreement the results were encouraging since they showed that structures with boroxol rings could be reproduced by introducing three-body potentials. This was due to a better reproduction of the B-O-B angles which were distributed around 120° in contrast to 160° encountered when pair potentials were used. In the wake of these works, Takada et al. [38] first and Cormack and Park [39,40] later developed and applied coordination dependent partial charge models with three-body interactions producing a higher number of boroxol rings (up to 53% of boron atoms engaged in such superstructural units in v- B_2O_3). However, the side effect was the significant underestimation of the density. On the contrary, when the simulations were performed keeping the density fixed at the experimental value a lower amount of boroxol rings formed and four-fold coordinated boron atoms were observed in the simulations.

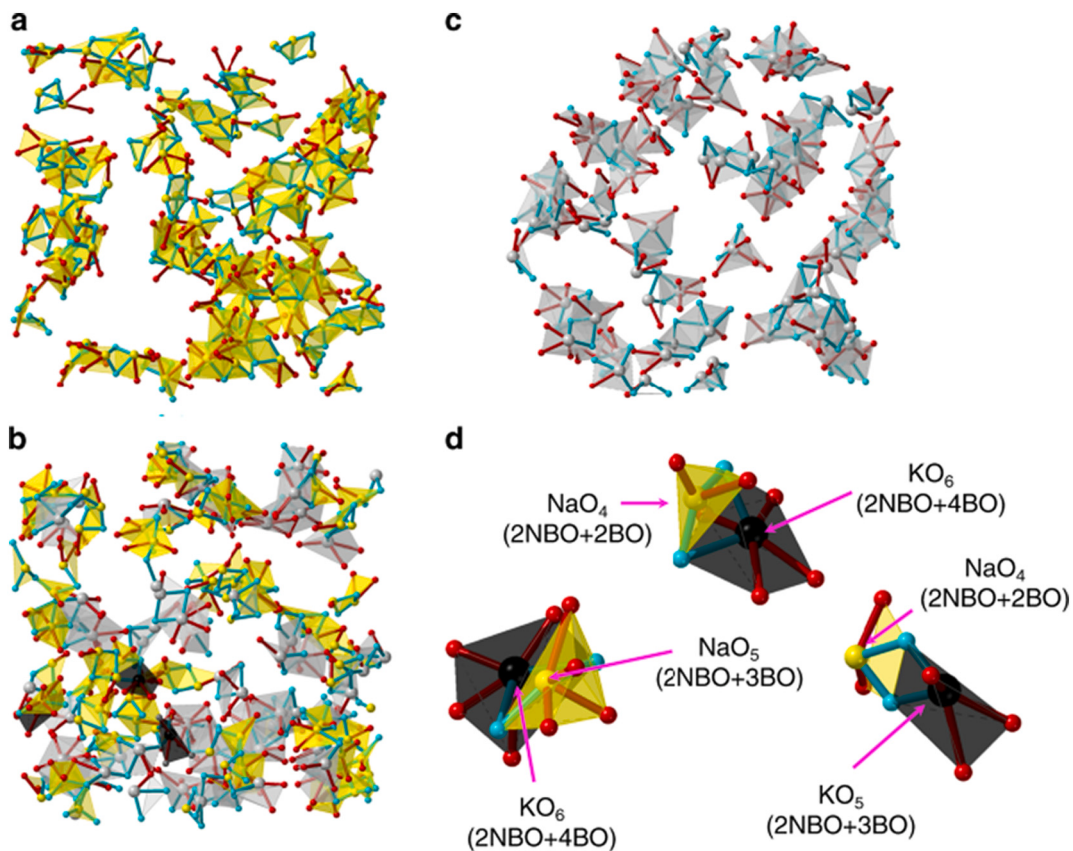


Fig. 1. The picture shows the percolation channels formed by the alkali polyhedra ($\text{Na} = \text{yellow}$, $\text{K} = \text{grey}$) in mixed Na, K silicate glasses with compositions $22.7\text{Na}_2\text{O}-77.3\text{SiO}_2$ (a), $11.35\text{Na}_2\text{O}-11.35\text{K}_2\text{O}-77.3\text{SiO}_2$ (b) and $22.7\text{K}_2\text{O}-77.3\text{SiO}_2$ (c). Panel (d) shows typical adjacent K and Na polyhedral forming bottleneck structures for the mobility of the two ions, which have different coordination environments. The picture has been taken from ref. [35]. (For interpretation of the references to colour in this figure legend, the reader is referred to the web version of this article.)

Until the end of the 80s, the parameters of the functional forms used to describe the interatomic interactions were derived empirically from atomic properties or by fitting against experimental data (crystal structures or correlation functions). However, the development of efficient software for quantum mechanical calculations soon allowed the production of reference data on cluster models of silica structures leading to the first QM-derived force-fields for silicates.

To the best of our knowledge, Tsuneyuki et al. [41] proposed the first QM-derived parameters in 1988 by fitting the Potential Energy Surface of model clusters of silica computed at the Hartree-Fock level of theory. They adopted a rigid ionic potential characterized by the sum of a Buckingham and a coulomb pair potentials:

$$U_{ij}(r) = \frac{q_i q_j e^2}{r} + A_{ij} e^{-r/\rho_{ij}} - \frac{C_{ij}}{r^6} \quad (6)$$

To describe the partial covalence of the Si-O bond partial charges of 2.4 and $-1.2e$ were assigned respectively to Si and O. This model is known by the acronyms of the authors: TTAM.

A few years later, van Beest et al. [42] showed that cluster calculations could not reproduce well the crystalline structure and properties of silica polymorphs and the inclusion of such macroscopic experimental data was fundamental. The well-known BKS potentials, which share the same functional forms and partial charges of the TTAM one, were then proposed.

These two potentials were widely used to study silica glass by many authors. [43–54] It was found that both potentials could reproduce fairly well the structure and several thermo-mechanical properties of various silica polymorphs and silica glass. A benefit of the employment of partial charges to model the partial covalence of the Si-O bond was the ability of both models to reproduce well the intratetrahedral O-Si-O

angle without the necessity of including three-body terms. The elastic constants were also in excellent agreement with experimental data with respect to the previous potentials that used formal charges and three-body interaction terms. However, the lack of any term accounting for lone pairs in the oxygen ions and their polarizability is probably the main cause for the overestimation of the intertetrahedral Si-O-Si angle. Albeit the BKS potential performed better, both potentials were not able to reproduce well the vibrational density of states (VDOS) in the complete IR spectrum. [55] It must be said that successive studies have shown that none of the simple rigid ionic models (comprising the ones developed later) can reproduce well the complete range of the vibrational spectrum. [56] This might be due to the lack of important polarizability effects [56–58] or simply because information on the VDOS was not taken into consideration during parameter fitting.

Despite their wide use, these potentials were not extended to multicomponent oxide glasses but were mainly used to study unary and binary oxide glasses. The TTAM potentials were extended to alkali silicate glasses by Habasaki et al. [59–61] using the same cluster approach and exploited by Heuer et al. [62–64] to study the structure, clustering, and dynamics of lithium ions in silicate glasses. Instead, the BKS potentials were extended to simulate the structure and dynamics of sodium silicate glasses. [65–67]

In the early 2000s, the knowledge acquired from the previous works on the benefits of using partial ionic charges was exploited to develop two sets of rigid ionic potentials models for multicomponent oxide glasses.

The first force field that appeared in the literature was developed by D.M. Teter. To the best of the corresponding author's knowledge, the original set of potentials was never published by Teter but communicated personally to Du and Cormack, which then modified and

extensively used them starting from 2003. [68–77] Teter's potentials are based on the pairwise terms reported in eq. 6 and used partial charges consistent with the BKS and TTMA potentials, that is, the charge of oxygen is $-1.2e$ and the cation charges scale proportionally from their formal charges to ensure charge neutrality of the overall system (Si: 2.4, P: 3.0, Al: 1.8, Ca: 1.2, etc). Following Du and Cormack's works the parameters have been modified by fitting on crystals and at the final potentials published until 2012 could cover silicates, phosphates, and aluminosilicates systems containing alkaline (Li, Na, K), earth alkaline (Ca, Sr) and rare earth (Y, La, Er, Eu, Ce) cations. Du and Cormack also developed a set of potentials to simulate hydroxyl groups in the bulk and on the surface of the glass surfaces. The complete set of potentials developed up to 2015 is reported in ref. [78]

Lately, Deng and Du also developed composition-dependent parameters to reproduce the partitioning between BO_3 and BO_4 units in borate and borosilicate glasses. [79] In particular, the A_{ij} parameter of the Buckingham functional form is a function of the maximum value of R ($=[\text{Na}_2\text{O}]/[\text{B}_2\text{O}_3]$), K ($=[\text{SiO}_2]/[\text{B}_2\text{O}_3]$), and N₄ (the fraction of BO_4 units) estimated by the Dell-Bray-Xiao model [80] for the glass of interest. This model has been shown to perform well in a wide range of compositions [81] but, as it will be discussed later on, it does not reproduce well the B-O-B bond angle distributions and the formation of superstructural features in borate glasses [82] as all the pair potentials models used in the 80s and discussed above. [3,5,11,12]

When the corresponding author of this manuscript started his Ph.D. internship in 2005 at the University of Modena and Reggio Emilia, he was asked to simulate the structure of phosphosilicate bioactive glasses to complement experimental data produced by internal collaborators and understand their properties. At that time, in our research group, we were still using models with full formal charges developed by Vessal and others described above, which however did not include P-O parameters. Therefore, since we were not able to find a completely self-consistent set of parameters for our systems of interest we decided to fit our own set of parameters. It must also be noted that a year before (during the holidays of 2004) the corresponding author worked for a few months in a company that produces polymeric film packages performing, among all, a lot of mechanical testing experiments on different polymeric formulations. This convinced him of the importance in the industry of such properties

and thus of the necessity of a set of parameters able to reproduce well also the elastic properties of multicomponent glasses.

Therefore, as done by Teter, we chose to use partial charges following the experience of the BKS potential but to describe the short-range interactions using a Morse function instead of the Buckingham one. We preferred the Morse function because of the more straightforward effect of the parameters on the potential curve (r_{ij} influences the minimum position, D_{ij} the depth of the well, and a_{ij} the curvature). A repulsive contribution of the form B_{ij}/r^{12} was also added to prevent atomic collapse at high temperatures and pressures. The functional form was

$$U_{ij}(r_{ij}) = \frac{q_i q_j e^2}{r_{ij}} + D_{ij} \left[\left(1 - e^{-a_{ij}(r_{ij}-r_{ij}^0)} \right)^2 - 1 \right] + \frac{B_{ij}}{r_{ij}^{12}} \quad (7)$$

where D_{ij} , a_{ij} and r_{ij}^0 are the parameters for the $i-j$ pairs of the Morse function, and B_{ij} is the parameter of the repulsive term acting at short distances.

The potential (often referred to as the Pedone or PMMCS potential) was parameterized to reproduce the experimental crystal structures and elastic constants of oxides, silicates, and aluminosilicates. [83] The complete set of parameters covers the elements highlighted in yellow in the periodic table reported in Fig. 2. Subsequently, we included the parameters for studying Vanadium [84] and Gallium [85] containing glasses and also the hydroxyl groups on silica surfaces [86], which are compatible with the hydroxyl-SPC water intermolecular parameters developed by Hassanali et al. [87]

The availability of parameters for a large number of cations-oxygen pairs and its ability to predict the mechanical properties fairly accurately have made it a popular choice for the study of the structure and properties not only of multi-component oxide glasses but also crystalline materials and oxide nanoparticles. [88–96]

In 2007, Guillet and Sator [97] published another simple force-field purposely developed for investigating the thermodynamics, structure, and transport properties of silicate melts made up of the nine geologically most abundant oxide components (SiO_2 , TiO_2 , Al_2O_3 , FeO , Fe_2O_3 , MgO , CaO , Na_2O , and K_2O). The Guillet-Sator (GS) FF shares the same functional form as the BKS, TTMA, and Teter ones but employed

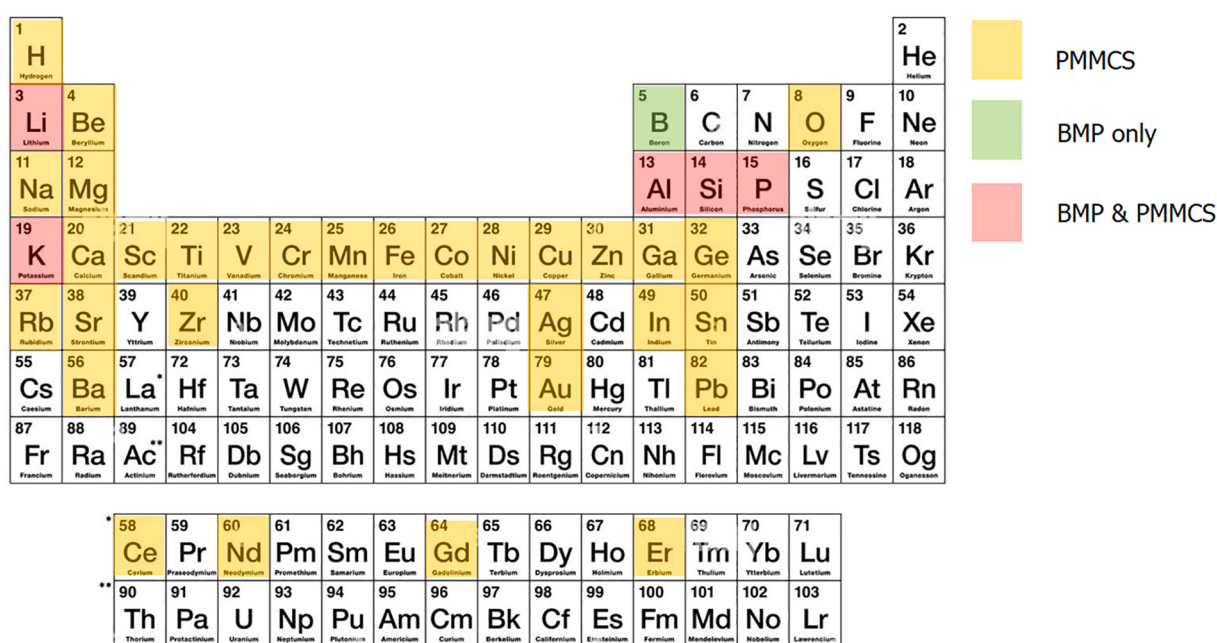


Fig. 2. Elements of the periodic table covered by the PMMCS (yellow and red), and BMP (green and red) potentials. The parameters of the PMMCS potential of the yellow elements are compatible with the parameters for the B, Al, Si, and P used in the BMP potential. (For interpretation of the references to colour in this figure legend, the reader is referred to the web version of this article.)

different partial charges consistent with a charge of $-0.945e$ for O.

The potential parameters have been determined by constraining the MD simulations to reproduce at best the density at zero pressure and the structure of a selected set of 11 natural silicate melts covering a large range of compositions (from felsic to ultramafic). As for the Teter and PMMCS FFs described above, it was assumed that cation–cation interactions are governed only by electrostatics (no short-range interactions have been included).

This model has been mainly used in the field of earth sciences to model magmatic melts [98,99] in order to find a relationship between macroscopic properties (molar volume) and microscopic structure (coordination of atoms) and dynamics as a function of the melt composition and pressure [100] but it has been also applied to aluminosilicate glasses. [101,102] In 2011, Kieu et al. [103] developed an empirical potential for sodium borosilicate glasses starting from the GS force field, using variable boron-oxygen interaction parameters. A few years ago, Wang et al. [104] also extended the GS potential to sodium and calcium borosilicate glasses. However, albeit this model is able to reproduce the BO_4 and BO_3 partitioning in borate and borosilicate glass with $R < R_{\max}$ (approximately 0.5–0.6) it fails above this value. [81] Again, no boroxol rings are observed in the generated structures.

Another interesting interatomic potential model is the one developed in 2018 by Sundaram et al. [105,106] which is known as the SHIK potential (from the authors Sundaram-Huang-Ispas-Kob). The SHIK potential has been firstly parameterized for pure silica and then extended to alkaline and alkali-earth silicate, aluminosilicate, borate, and borosilicate glasses. [107]

It is a pairwise interatomic potential in which the long-range electrostatic interactions are evaluated by means of the Wolf truncation method [108], whereas the Buckingham functional form is used for the short-range interactions:

$$U_{ij}(r_{ij}) = U_{ij}^W(r_{ij}) + A_{ij}e^{-\frac{r_{ij}}{r_{ij}^W}} - \frac{C_{ij}}{r_{ij}^6} + \frac{D_{ij}}{r_{ij}^{24}} \quad (8)$$

where

$$U_{ij}^W(r_{ij}) = z_i z_j \left[\frac{1}{r_{ij}} - \frac{1}{r_{cut}^W} + \frac{(r_{ij} - r_{cut}^W)}{(r_{cut}^W)^2} \right] \quad (9)$$

r_{cut}^W is the cutoff for Coulomb interactions. The cation charges are fixed, whereas the oxygen charge depends on the glass composition.

The parameters of the FF have been determined to reproduce the pair distribution functions evaluated by ab initio MD simulations of melts of silicate [105,106] and aluminosilicate [106] systems at high temperature and were widely used by the inventors to study fracture mechanisms and elastic properties in sodosilicate glasses. [109,110]

Of course, the availability of all the aforementioned interatomic potentials has boosted the application of MD simulations to study the structure and properties of oxide glasses in a wide range of compositions.

The main limitation of all the rigid ionic models described so far is the poor reproduction of the Q^n distributions (Q stands for quaternary species whereas n is the number of Bridging oxygens bounded in the first coordination sphere) of silicon species in silicate glasses, which are broader than the experimental ones. As it will be recalled in the next section on the polarizable interatomic models, Tiloccia was the first to realize that improved Q^n distributions were obtained by employing the core-shell model proposed by Dick and Overhauser [111].

The simulation of solid-state NMR spectra of several spin active species (^{29}Si , ^{11}B , ^{17}O , ^{27}Al , etc....) of multicomponent oxide glass structures produced with the rigid ionic models and the shell model using the MD-GIPAW approach that we have proposed together with Charpentier [112–114] demonstrated that the latters were more reliable and in agreement with experiments. [89,114–121]

The shell model not only reproduced better the Q^n distribution but also narrower Si-O-Si bond angle distributions centered at smaller

angles. Indeed, several theoretical investigations had already revealed that a direct correlation between the ^{29}Si isotropic chemical shift and the Si-O-T bond angle ($T = \text{Si}, \text{Al}, \text{B}$) existed. [89,122] This suggested that there could be a correlation between the bond angle distribution and Q^n species distributions. Moreover, Lodesani et al. [102] showed that among the PMMCS, SHIK, Teter, GS, and core-shell model only the latter was able to reproduce correctly the Mixed Alkali Effect on ionic conductivity of sodium potassium aluminosilicate glasses. This was attributed among other structural features to the narrower inter-tetrahedra Si-O-Si angle that translates to the formation of larger rings and percolation channels accommodating the alkaline ions with respect to the rigid-ion model. Within such channels, sodium and potassium seem to locate randomly but in different local environments obstructing each other mobility when they are equally mixed. Another intriguing behavior observed was that the ionic conductivity of potassium aluminosilicate glasses was higher than that of sodium aluminosilicate ones only at high temperatures. This was also attributed to the formation of larger rings which are more flexible and can expand more easily at high temperatures with respect to the smaller ones. The rigid ionic models evaluated, developing different (larger and broader) bond angle distributions and ring size distributions were not able to reproduce the right trend of the ionic conductivity.

To overcome these limitations and also to resolve some issues in the PMMCS potentials observed during the years (overestimation of the density) [123] we revisited recently the original model by including *i*) a T-O-T ($T = \text{Si}$ and P) three-body interactions, described by screened-harmonic functional forms (see eq. 11 in the next section); *ii*) Si-Si, Si-Al, Si-P, Al-Al, and P-P repulsive interactions; and *iii*) refining Li-O, K-O, and P-O pair-wise parameters using DFT reference data. [124] The new FF, named BMP (from Bertani-Menziani-Pedone), reproduces density, structure (Bond Angle Distributions, Q^n species), and properties of silicates, aluminosilicate, phosphate, and phosphosilicate glasses significantly better than the original model as shown in Fig. 3.

Recently, our new FF has been also extended [126] to borate and borosilicate glasses by developing a composition-dependent model to compute the D parameter of the B-O pair interaction. It has been applied to a wide range of glass compositions and tested on experimental data such as the fraction of BO_4 (N_4), density, non-bridging oxygen (NBO) speciation, neutron diffraction spectra, ^{11}B , ^{29}Si , and ^{17}O MAS NMR. Fig. 4 reports a comparison of the percentage of BO_4 units in borate glasses, neutron structure factors, and ^{11}B MAS NMR spectra in borosilicate glasses obtained with the BMP and other interatomic potentials available in the literature. Although the B-O-B angle distribution is narrower than the pair-wise potentials described above it is centered at 130° and thus only a negligible amount of boroxol rings are observed in MD-derived structure of v- B_2O_3 .

2.2. The polarizable interatomic models

The interatomic potentials presented so far made use of rather simple functional forms not accounting explicitly for polarization effects, charge redistribution during dynamics, and bond breaking.

Regarding the inclusion of polarization, two models were available in the 90s. The shell model approach devised by Dick and Overhauser [111] and widely used in lattice dynamics calculations of points defects and structures of oxides and inorganic materials, [21,127,128] and the Polarizable Ionic Model proposed by Madden and Wilson. [129]

In the core-shell model, the Born-Mayer ionic model is still used but the most polarizable ions (O^{2-} in oxide systems) are split between a core bearing almost all the mass and a positive charge, X , and a shell bearing a negative charge, Y ($X + Y = Q$, the formal charge). The core and shell of the polarizable ions are screened from Coulomb interactions and coupled by a harmonic spring potential of the form:

$$U_{c-s}(r) = \frac{k_{c-s}}{2} (r_{c-s})^2 \quad (10)$$

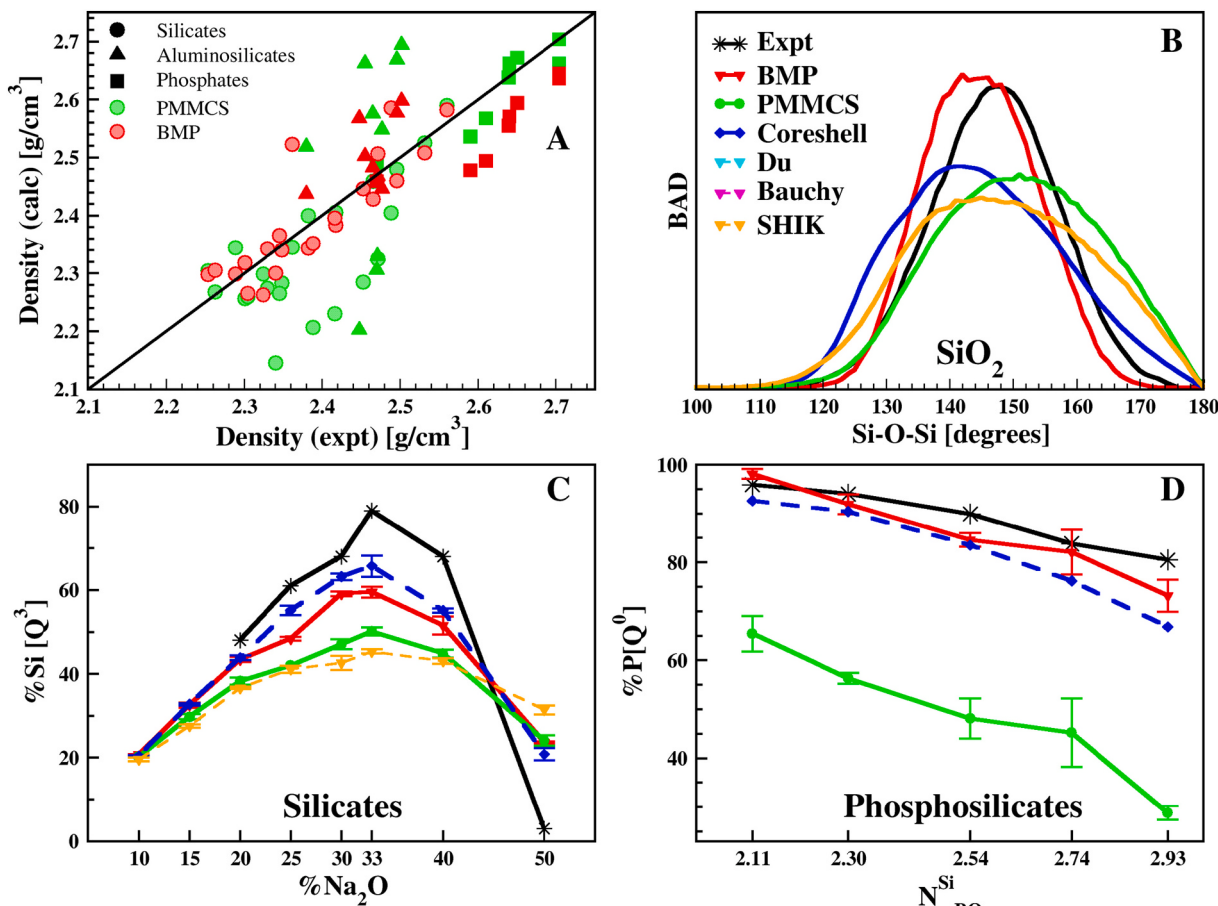


Fig. 3. (a) Correlation plot between the experimental and calculated densities of alkali silicates, aluminosilicate, Na, Ca- phosphate, and phosphosilicate glasses investigated in ref. [124] using the PMMCS (green symbols) and the BMP (red symbols) potentials. (b) Comparison of the Si-O-Si Bond Angle Distributions in v -silica computed using different interatomic potentials with the experimental one extracted from ^{29}Si NMR experiments; [122] (c) Percentage of Q^3 species as a function of Na_2O content in binary sodium silicate glasses; (d) trends of the Q^0 species for phosphorous in phosphosilicate glasses with different network connectivity (average number of Bridging Oxigens per silicon atom) for BMP, PMMCS and CS parameterizations by Stevensson et al. [125]. (For interpretation of the references to colour in this figure legend, the reader is referred to the web version of this article.)

Where k is the force constant of the spring and r_{c-s} is the distance between core and shell. Usually, the charge splitting and the spring constant are determined to reflect the polarizability of the anions. [130] The total energy is made up of pair potentials (where the short-range interactions between shells are modeled with a Buckingham potential, while long-range core-core, core-shell, and shell-shell electrostatic interactions are modeled with a Coulomb potential) and three-body terms for the proper description of intra-tetrahedral O-T-O angles ($\theta_{ijk}^0 = 109.7^\circ$). A screened harmonic potential (eq. 11) is used most of the times:

$$U(\theta_{ijk}) = \frac{k_b}{2} \left(\theta_{ijk} - \theta_{ijk}^0 \right)^2 \cdot \exp \left(-\frac{r_{ij}}{\rho_b} - \frac{r_{ik}}{\rho_b} \right) \quad (11)$$

Despite the success of this model in studying dielectric properties and defects in oxide ceramics it was not used to simulate oxide glasses until 2006. [131] Tiloccia et al. extended the Sanders and Catlow Si-O and O-O potentials to study sodium and soda-lime silicate glasses [131] and the bioactive glasses of the soda-lime phosphosilicate family. [132–134] As already anticipated, the structure of glasses simulated with this approach was found to be in better agreement with NMR experiments in terms of Silicon and Phosphorous Q^n distribution with respect to the rigid ionic model. [135] This model was later extended and used in our group to study mixed oxyhalide glasses, [130] Mg-, Ga- and Ce-containing bioactive glasses, [85,136–139], and sodium-calcium aluminosilicate glasses. [115,116,140] We found that the simulated

solid-state NMR spectra of spin active nuclei (such as ^{17}O , ^{29}Si , ^{27}Al , ^{31}P , etc....) using structural models generated using the shell model were in good agreement with experimental counterparts because of the better Q^n and T-O-T bond angle distributions (T = network former ions). Recently, Stevensson et al. [125] extended this model for borate and borosilicate glasses finding that it accurately reproduces boron coordination in a wide compositional space without resorting to composition-dependent B-O parameters. [82,141,142] As for the formation of boroxols and other superstructural units we noticed a small amount of them with respect to that expected experimentally. [126]

Despite the great improvements provided by the inclusion of polarizability this model has not been as widely employed as one could expect. This is probably due to the high computational cost required to perform MD simulations. Two approaches can be used: the dynamical and the relaxed shell model. In the first approach, a fraction (x) of the atomic mass (m) is applied to the shell and its movement is described by the classical equation of motion as for the other particles in the systems. The mass of the shell is chosen to ensure that the natural frequency of vibration ν of the harmonic spring

$$\nu = \frac{1}{2\pi} \left[\frac{k}{x(1-x)m} \right]^{1/2} \quad (12)$$

is well above the frequency of the whole atom in the system in order to avoid the effective exchange of kinetic energy between the core-shell units and the remaining systems. This also requires the employment of

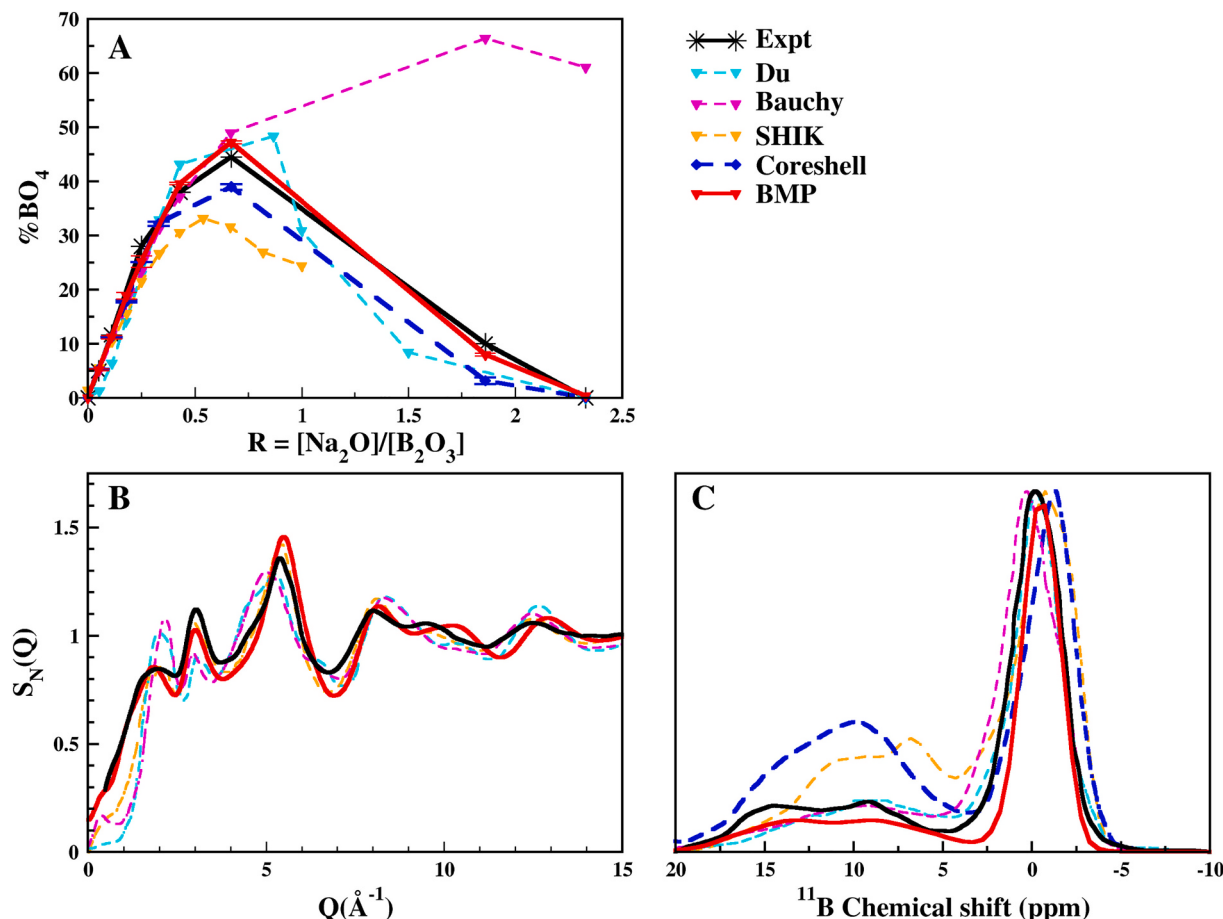


Fig. 4. (a) Percentage of BO_4 units as a function of the ratio $R = [\text{Na}_2\text{O}]/[\text{B}_2\text{O}_3]$ for borate glasses; (b) neutron structure factors for the $0.8\text{Na}_2\text{O} - 3.8\text{SiO}_2 - \text{B}_2\text{O}_3$ glass and (c) ^{11}B MAS NMR spectra of the $1.36\text{Na}_2\text{O} - 3.07\text{SiO}_2 - \text{B}_2\text{O}_3$ glass obtained using different interatomic potentials.

timesteps at least 1 order of magnitude smaller than that used for the rigid ionic model. Instead, in the relaxed shell model, the shell positions are minimized after each MD step. This allows for using longer timesteps but still extra steps are necessary to equilibrate the shell positions. Aside from the additional computational cost, the dynamical shell approach is more difficult to manage, simulations in the NVT ensemble and rescaling the velocities of the shell every few steps are usually necessary to avoid temperature explosion and the escape of the shell from its core. Beyond these computational problems, it must be emphasized that the current parameterizations are not accurate to model important properties such as density and mechanical properties [124] but this is because the parameters have been fitted using only information on the structure of crystals.

The Polarizable Ionic Model (PIM) allows to explicitly account for the many-body polarization effects [143]. This model is composed of four terms: electrostatic (charge-charge), overlap repulsion, dispersion, and polarization. The first three terms are two-body terms and the dispersion one is made by dipole-dipole and dipole-quadrupole interactions, with a short-range correction obtained with Tang-Toennies damping functions. [144,145] The polarization term includes dipolar and quadrupolar contributions and the charge-dipole and charge-quadrupole interactions are also corrected for the short-range penetration using Tang-Toennies damping functions. The full functional forms are complex and would require a lot of space to be reported and described. Therefore, we remand the interested reader to more specific manuscripts. [129,146–149] The main advantage of this model is the better reproduction of the dipole induction by the coulomb and short-range interactions with respect to the core-shell one. The polarization effect can, in fact, be parameterized unambiguously by ab-initio

electronic calculations. The PIM approach has not been widely applied for the simulation of oxide glasses due to its complex nature which makes it very complicated to be parameterized and it has not been extended to many elements, lacking in transferability. Furthermore, the majority of the most used MD programs (DL_Poly [150], LAMMPS [151], ...) do not allow to use this model. To our knowledge, the applications were limited to the simulation of SiO_2 [58,152], GeO_2 [153], B_2O_3 [154], and Na-borosilicate [149] amorphous systems leading to a good computation of vibrational spectra and allowing to stabilize the formation of boroxol rings in B_2O_3 , producing $\sim 33\%$ of rings, better than other force fields.

2.3. Reactive force-fields

The potential models described in the previous paragraphs can be used to simulate the structure and several bulk properties for glass oxides of many compositions.

However, they are not suitable to investigate the chemical reactivity of these systems, due to the invariability of the potential parameters on the chemical environment and the simplicity of the functional forms, which cannot describe accurately bond breaking and forming. The accurate description of reactions' events requires the use of *ab-initio* simulations, which are quite expensive computationally.

Albeit in the last years we have witnessed a huge improvement in the computational power and efficiency of algorithms, *ab-initio* molecular dynamic (AIMD) simulations are still limited to systems of modest size (few hundreds of atoms) and short time length (hundreds of ps).

Reactive potentials were developed to overcome these shortcomings. The main ingredient of the models proposed is the dependency of the

covalent terms by bond orders or coordination states, which are computed on the fly at each step of the simulations based on the pair bond distances. Therefore, the molecular connectivity can change, mimicking the quantum mechanical potential energy surfaces, which are typically used in the fitting of the parameters.

The first form of bond order potential was proposed by Tersoff [155] for silicon: the covalent interaction was described by a Morse potential, where the bond strength parameter was dependent on the local environment. This model was capable of reproducing different silicon structures, including specific features of the surfaces. Despite the room for improvement, this functional form was considered capable of capturing the essential physics of covalent bonding and provided a starting point for subsequent developments in reactive force fields [156].

Huang and Kieffer [157] developed a coordination dependent charge-transfer three-body potential characterized by the dynamical redistribution of atomic charges which controls the extent of charge polarization in covalent bonds; two and three-body interactions dependent on the degree of covalency and the actual coordination numbers of the atoms involved during the interaction. They investigated the structural and thermomechanical properties of crystalline and amorphous SiO_2 and B_2O_3 within different T and P regimes reproducing accurately the coordination changes of the Si and B under pressure. [157–159] To the best of our knowledge, this model was not extended to multicomponent oxide glasses nor to include water interactions.

Garofalini and coworkers pioneered the field of reactive simulation at the silica-water interface by developing a dissociative multibody potential, with both pair and three-body terms, for the study of silica and silica/water interaction. [16,160,161] With their potentials, they were capable to elucidate the hydroxylation of the surface, which involves water adsorption, siloxane bond breaking, and silanol formation. [160] Successively, with a newly developed dissociative water model, [162] they found a concentration of Si-OH groups comparable with the experimental values. [163] In the same work, they observed the formation of hydronium ions from water interacting with silica, in agreement with the results from AIMD simulations. A more recent and refined potential was then used to elucidate the proton diffusion on amorphous silica/water interphase, differentiating the lifetime of the protonated species H_3O^+ , SiOH , SiOH_2^+ and $\text{Si}(\text{OH}^+)-\text{Si}$, and finding a faster proton diffusion on the silica than in bulk water, in agreement with electrochemical studies. [164] The same potential was adopted to study the silica surface dissolution in water, by characterizing the hydrolysis of the different Q^n species with the associated barriers, which were found to lie near the low-end of the experimentally measured range. The study found that the rate-limiting steps were the transition from species Q^3 to Q^2 and from Q^2 to Q^1 , and the key factors in regulating the different barriers were the degree of distortion of the tetrahedral units and the accessibility of water molecules to the reaction sites. [165]

Among the reactive potentials developed so far, the ReaxFF model, originally developed by van Duin and coworkers for the study of hydrocarbons in 2001, [166] is quickly spreading in the glass science community to study the first stages of glass dissolution in water and the structure of the alteration gel formed at silica surfaces upon its interaction with water. [167,168]

In ReaxFF the energy of the system is partitioned in the sum of partial energy contributions, as shown in eq. 13:

$$E_{\text{system}} = E_{\text{bond}} + E_{\text{over}} + E_{\text{under}} + E_{\text{val}} + E_{\text{tors}} + E_{\text{pen}} + E_{\text{conj}} + E_{\text{vdWaals}} + E_{\text{Coulomb}} \quad (13)$$

The first 5 terms are all dependent on the bond order and are respectively the terms for the bonding (E_{bond}), the over-coordination (E_{over}), the under-coordination (E_{under}), the valence angle (E_{val}), and the torsional angle (E_{tors}). System-specific terms include a penalty contribution (E_{pen}) for systems with cumulated dienes, and a stabilizing conjugation contribution (E_{conj}) to the energies for systems with

conjugates ones. Then, the non-bonding contributions are described by the remaining terms: the Pauli's repulsion and the dispersion attraction energies are included in the van der Waals term (E_{vdWaals}), and the electrostatic interactions are described by the Columbian one (E_{Coulomb}).

The analytic functional forms are quite complex and are not reported here for the sake of simplicity. The interested readers can refer to the original paper. [166]

We report here only the functional forms used to compute the bond order which is calculated on the fly, at each step of the simulation, from the interatomic distances using the following equation:

$$BO_{ij} = BO_{ij}^\sigma + BO_{ij}^\pi + BO_{ij}^{\pi\pi} \\ = \exp \left[p_{bo1} \left(\frac{r_{ij}}{r_0^\sigma} \right)^{p_{bo2}} \right] + \exp \left[p_{bo3} \left(\frac{r_{ij}}{r_0^\pi} \right)^{p_{bo4}} \right] + \exp \left[p_{bo5} \left(\frac{r_{ij}}{r_0^{\pi\pi}} \right)^{p_{bo6}} \right] \quad (14)$$

BO is the bond order (it should not be confused with Bridging-Oxygens) between the atom pair i and j which is partitioned in sigma and pi greek bonding type contributions (the latter are neglected in oxides), r_{ij} the interatomic distance, r_0 is the parameter for the equilibrium bond length, and the p_{bo} terms are other empirical parameters [169].

The non-bonding interactions are computed between all atomic pairs of the system, including the bonded pairs, to avoid discontinuities in the energy during the dissociation/formation of bonds. Additionally, atomic charges are computed dynamically adopting the Electron Equilibration Method (EEM) approach, [170] which makes it possible, at least in principle, to describe redox reactions or charge separation processes.

The first reactive potential of interest for oxide glasses was first developed for the study of silicon-silicon oxide interfaces. [171] The parameters were fitted using a quantum mechanical training set of structures, energy barriers for the Si-O bond-breaking, and the equation of states for the crystalline phases of Si and SiO_2 .

The structure of silica glass and its properties such as the elastic constants and self-diffusion computed with ReaxFF have shown to be in good agreement with experimental data. [172]

The most interesting applications of reactive force fields for the study of reactivity of oxide glasses involve the simulation of the silica/water interface and the properties and reactions occurring at the alteration layer at the glass surface that forms following glass hydroxylation, dissolution, and re-precipitation phenomena. Other phenomena of huge interest occurring in presence of water are the ionic exchange, crack propagation, and the chemical and mechanical polishing of glass surfaces.

The first water-silica glass investigation performed with ReaxFF provided a similar description of the hydroxylation of the silica surfaces, but no siloxane hydrolysis was reported [173]. Instead, a Grotthuss-like mechanism of diffusion of the proton in the glass network was observed. In subsequent studies, the Si/O/H ReaxFF potential parameters were refined including in the fit also the energy barriers of the hydroxylation reaction of strained and not strained Si-O structures computed at the DFT level providing improved results. [174,175] An example of the mechanism observed for the hydroxylation of a strained siloxane bond is shown in Fig. 5.

ReaxFF parameterizations of Si/O/H were further tested on the DFT energies of the hydroxylation of silica nanoparticles of different sizes and amounts of hydroxyls. The energetics at high and intermediate degrees of hydroxylations were well reproduced, whereas worse results were found at the lower degree. [176]

Mahadevan et al. [177] compared the Garofalini reactive potential with the first ReaxFF parameterization for Si/O/H finding that the former describes generally better the properties of amorphous silica, water, and the silica/water interface, despite adopting a simpler potential. At the time of the comparison the new and more accurate parametrization of the ReaxFF for water [178] was available, but not used.

Since its success, the Mahadevan and Garofalini reactive potential for

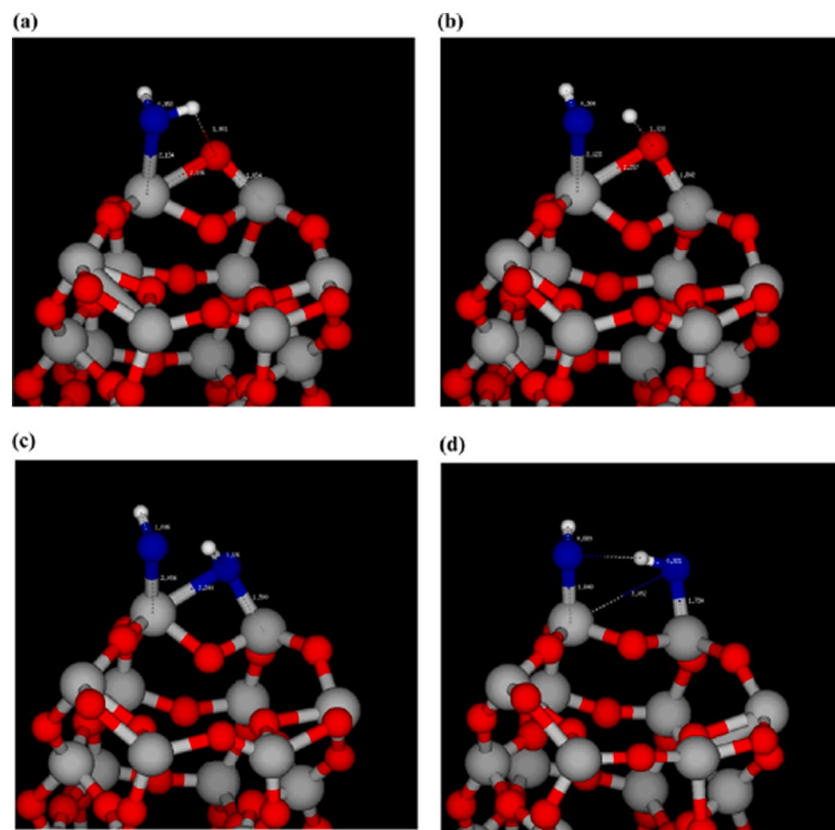


Fig. 5. Snapshots of the hydroxylation reaction of an adsorbed water molecule at 1500 K on a nano-silica structure, as reported in Yeon and van Duin [174]. The color code use grey for Si, white for H, red for O atoms not bonded to H, and blue for O atoms bonded to H. It is shown, starting from a water molecule adsorbed on a Si of strained ring structure (a), the transfer of H to a bridging oxygen (b), which is first protonated (c), then the Si-O bond breaks, to form two vicinal silanols (d). Reprinted (adapted) with permission from Yeon and van Duin.[174]Copyright {2016} American Chemical Society. (For interpretation of the references to colour in this figure legend, the reader is referred to the web version of this article.)

water and silica was further extended to describe sodium, aluminum, and calcium silicates. [179–181]

Similarly, also ReaxFF was further parametrized to describe sodium silicate, [182–184] aluminosilicates [185], and their interaction with water. [184]

ReaxFF-MD simulations have been extensively carried out in the last years by Du's group to investigate key steps in the formation of the alteration layer at the glass surfaces in water, such as silica dissolution and silica-gel formation [167,168], the leaching from sodium silicate [186] and sodium aluminosilicate glasses, [183,187,188] and the water induced fracture. [189–191]

Fig. 6 shows the interfacial models that consist of bulk silica, nanoporous hydrated silica gel, and bulk water constructed by Rimzsa and Du in one of their first investigations of the silica gel structure and dynamics. [167] They observed an increase in Si–O network connectivity with time in the gel region as a consequence of the cross-linking of siloxane bonds in the gel and the dissolution of less connected [SiO₄] groups into the water region. The polymerized silica gel was suggested to passivate the glass surface and regulate the transport of ions and further glass dissolution.

Another interesting application of ReaxFF in the context of glass reactive studies is the simulation of the chemical mechanical planarization (CMP), a process of smoothing of the surfaces which exploits the combined action of mechanical abrasion and tricochemical reactions during the friction between surfaces. Many studies have been performed adopting silica glass as either abrasive material or as the surface to be polished, investigating the effects of the humidity, the contact pressure, and the presence of chemicals such as H₂O₂ on the efficiency of the process, typically evaluated by the number of atomic species removed by the abrasive surface. [192–195]

Albeit ReaxFF is a powerful tool to simulate glass reactivity some limitations have been observed. Firstly, most of the libraries available have not been parametrized for simulating the melt phases and the glass structures generated are usually of worse quality with respect to that

obtained with the rigid ionic potentials described above. For example, several tests performed in our group (whose results have never been published) showed that aluminum coordination in aluminosilicate glasses is badly reproduced with all the ReaxFF parameterizations available at the time of writing. Moreover, it has been shown in several studies that at high temperature molecular oxygen is formed and persist also at lower temperature affecting the final structure. [196] This problem can be avoided by deactivating the bond-order O–O during the annealing process. [196]

Another limit of the ReaxFF lies in the methodology to compute atomic charges. The EEM method, [170] in fact, works well to describe chemically reasonable structures near the equilibrium [197,198], but it may result in unrealistic charge distributions for geometries far from the equilibrium, as can be encountered when generating the glasses structures from melt phases of the glasses and in the quenching.

Another issue is the incorrect description of dispersion interactions. This is probably due to the fact that ReaxFF parameters are typically trained on DFT data obtained with functionals which usually underestimates or neglects the London forces, the attractive component in vdW interactions.

Albeit these contributions might be less important for the bulk structure of oxide glasses they can play a role in the surface reactivity. Remedies to this problem, other than the use of more accurate *ab-initio* training datasets, is the introduction of corrective terms into Reaxff for the description of long-range London interactions only, such as the low-gradient correction (Reaxff-lg). [199]

A major issue in the application of ReaxFF to oxide based glasses is the lack of extended parameterizations for multicomponent glasses. Most of the ReaxFF parameters are trained on the crystalline structures of single component oxides, not even on amorphous phases, possibly limiting the transferability to the glass phase or to extended regions of compositions. The situation is even more involved for multivalence species such as B, P, V, Ce, etc....

All these problems make the development of ReaxFF libraries of

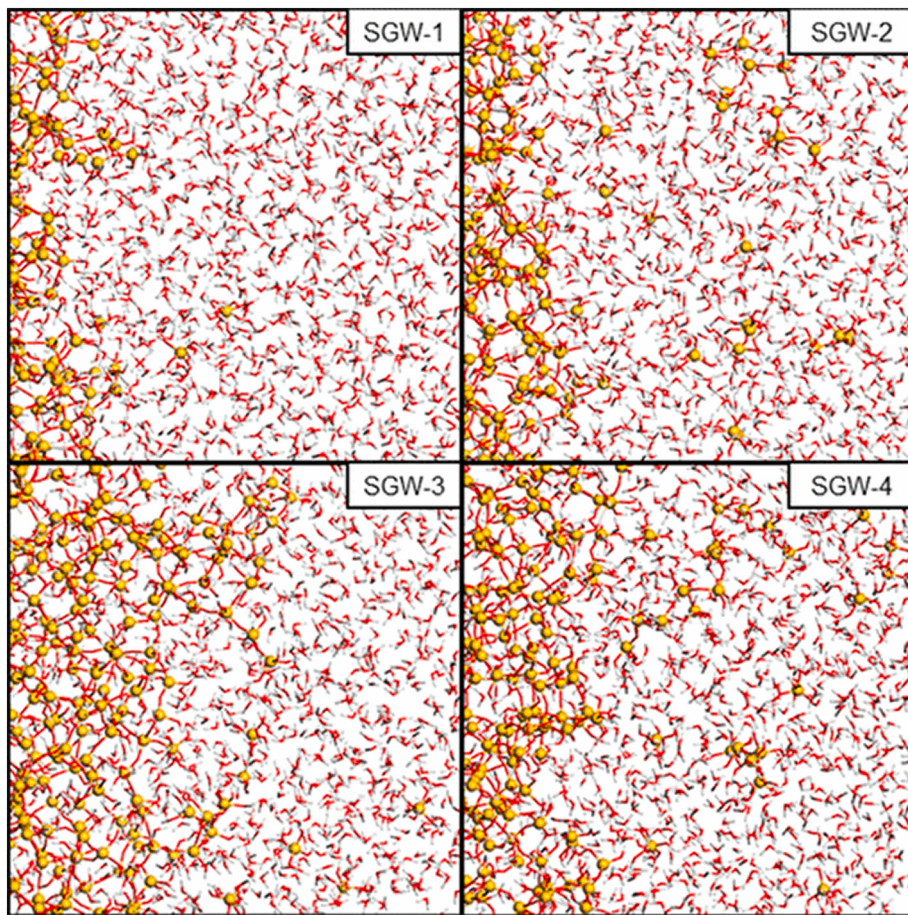


Fig. 6. Snapshots of evolving gel–water interface and dissolved silica in the water region for the Silica–Gel–Water (SGW) model structures generated by Rimsza and Du. [167] SGW-n models have been obtained by using different annealing temperatures (300, 500, 700, and 900 K). Colors: oxygen (red), silicon (yellow), and hydrogen (white). MD simulations 1 ns long reveal a gradual growth of the gel region into the water, resulting in the dissolution of silica into the water from the gel, while the dense silica remains intact at these temperatures and time ranges. Reprinted (adapted) with permission from Rimsza and Du. [167] Copyright {2017} American Chemical Society. (For interpretation of the references to colour in this figure legend, the reader is referred to the web version of this article.)

potentials to describe the chemistry of multicomponent glasses an extremely demanding task.

3. Practical considerations on force-fields parameterizations

The development of force fields (functional forms and parameters) is a quite complex task and should be approached following several steps and more importantly taking into proper consideration the peculiarity of the systems and properties that one wants to simulate. On the basis of the final aim of the force fields, one should first choose the proper interatomic potential model and functions or propose new ones. For, example, if the final aim is to reproduce the dielectric properties of the materials the rigid ionic model is clearly not a good choice since ionic polarizability is fundamental to reproduce it. Analogously, if the interest is the chemical reactivity of glass surfaces a bond-breaking model is mandatory whereas if the interest is on the structure and elastic properties the rigid ionic model with proper functional forms is sufficient.

Having defined the model and the functional forms, the following step is to obtain its parameters among which the ionic charges are included. This step can be succeeded by fitting them to reproduce known experimental or *ab initio* data. In the former case, we usually talk about empirical fitting.

Despite the choice of the reference data this step consists of the minimization of a cost function quantifying the distance of the results (observables) obtained with a set of parameters with the target ones.

A typical cost function is the sum of squares function F defined as follows:

$$F = \sum_{i=1}^M w_i (f_{i,obs} - f_{i,MM})^2 \quad (15)$$

Where M is the total number of observables used during fitting, w_i is a

weighting factor for each observable and $f_{i,obs}$ and $f_{i,MM}$ are the target (experimental or QM-computed) and the MM-computed observables, respectively.

Any computable property of a crystal, cluster, or amorphous structure could be used. Obviously, the structural properties are mandatory since the property calculations must be carried out on the right structure. Therefore, generally, the structure (lattice vectors and positions) of crystalline solids are used and other properties such as elastic constants, dielectric and piezoelectric constants, lattice energy, vibrational frequencies, or dynamic properties can be added if available.

The reproduction of these quantities ensures the right reproduction of the stable minima and related curvatures present in the potential energy surface of the system of interest. The position and depth of the potential well largely determine bond length, density, and defects formation energy, while the shape of the minimum affects atomic vibrations and elastic moduli.

Empirical fitting is usually distinguished in the conventional and relaxed fitting. In the former, the forces on the experimental atomic structure are minimized (they should be zero) and the properties are computed on the experimental/reference structure. However, this method is not adequate because reducing the forces does not guarantee a good optimized structure since the displacement in geometry optimization (with the Newton method) is given by the gradients multiplied by the inverse hessian matrix and if forces are small but the inverse hessian is much higher the displacements on the geometry can be very high leading to erroneous structures.

To solve this problem and to succeed in obtaining the right structure and good properties computed in the MM optimized geometry as it should be, the so-called ‘relaxed’ fitting method introduced by Gale [200] in 1996 can be performed. In this case, the accuracy of a potential

model is evaluated from the displacements of the optimized structure away from the experimental configuration. The structure is therefore optimized at every step of the parameter optimization and the displacements of structural parameters are calculated instead of the energy gradients [83]. Moreover, it is possible to fit to many structures at the same time, to improve the transferability of the fitted variables and minimize errors [200].

It is worth to discuss how to choose the weighting factors appearing in eq. 15 since their variation leads to an infinite number of possible solutions of the minimization problem which are equally valid from the mathematical point of view but not from the physical one. Therefore, one of the fundamental skills of a good force-field developer is to know how to choose appropriate and sensible weighting factors. The criteria to follow are:

- 1) if the fitting is performed on experimental data, the weights should be inversely proportional to the uncertainty in the measured value.
- 2) the weighting factors should be inversely proportional to the magnitude of the observable squared. This ensures a more balanced fit, that is, all values are fitted on an equal footing, regardless of units. In other words, they should be chosen so that the contribution to the overall error of the individual observables used in the cost function is approximately the same.

Most of the potential models (especially the earlier ones) were usually parameterized by fitting to experimental data [1,16,49,83,97].

The limitations of this approach derive from the availability of large datasets for both structure and properties and the uncertainty associated with the measured properties. Therefore, this approach is limited to crystalline bulk structures since the atomic positions for amorphous structures are not available.

Moreover, since the majority of the experimental data are usually measured at room temperature when the system fluctuates only near the minimum of the potential energy surface the parameters might not be transferable at higher temperatures where the system can explore different regions of the PES.

Despite these limitations, empirical fitting is still widely used and most of the potential models discussed above (Du, Guillot and Sartor, PMMCS and BMP, and most of the core-shell potentials) exploited this approach.

The fitting on quantum mechanical data became increasingly important at the end of the 1990s in deriving potentials [41,42], thanks to the availability of several quantum mechanical codes based on density functional theory which made possible the computation of the structure and properties of molecules, materials, and surfaces for which experimental data are not available.

In earlier works, the fitting was performed against *ab initio* calculations of small clusters and the parameters used to study SiO₂, GeO₂, and B₂O₃ glasses [41,154,201,202]. However, the parameters were not able to reproduce well bulk structures and properties and thus, in several cases, the inclusion of experimental bulk properties data was still necessary [42]. This problem was overcome by exploiting periodic DFT calculations to compute structure and properties (elastic constants and frequencies) as we have done in the past for silica polymorphs and their surfaces or hydroxyapatite. [57,203]

Car-Parrinello [204] (CPMD) and Born-Oppenheimer MD (BOMD) simulations [205] can provide very accurate data on the local structure and electronic properties of silicate glasses and for this reason, they are nonetheless very useful to provide *ab initio* data on the short-range local structure of glasses, which are difficult to obtain experimentally.

Indeed, some potentials for former oxides only, are fitted on some *ab initio* MD simulations on bulk systems such as the CHIK potential [206], developed by Carrè et al. firstly on silica and then extended to oxide glasses by Sundaram et al. [105,106].

The SHIK potential [105,106] has been parametrized using the radial distribution functions of the liquid silicates computed from BOMD

including also experimental data on properties such as the Young modulus, density, and (for borates) the percentage of the BO₄ units of the glass.

In the conclusion of this section, we would like to discuss the methods used to minimize the cost function.

Being an optimization problem the usual BFGS [207] or the Levenberg-Marquardt algorithms [208] can be used when the analytical or numerical derivative of the sum of square function with respect to the force-fields parameters are available,

When this is not the case machine learning methods can be exploited. For example, Bayesian optimization [209,210] has been used in several recent works. This is a machine learning-based approach that tolerates stochastic noise in function evaluation and that quickly optimizes a black-box objective function over a continuous domain of fewer than 20 dimensions.

The first step is to evaluate the objective function with respect to an initial space-filling experimental design that often consists in choosing random and uniform points within a defined domain. Secondly, a surrogate function for the objective that quantifies the uncertainty using Gaussian Process Regression [211] (GPR) is built. Thirdly, an acquisition function is defined from this surrogate, and it is used to decide where to sample the next point. The last step is the evaluation of the real objective function and the update of the surrogate one. The process is iteratively repeated a number of times decided by the user. Examples of this new approach are given by Liu et al. [210] for silica in 2019, Urata et al. [213] for lithium borate and borosilicate glasses in 2022, and, by Bertani et al. [126] for borate and borosilicate glasses.

4. Future developments: Machine-Learning FFs

In the last decade, the development of efficient Machine Learning algorithms and the availability of a large mole of data has led to a pervasive application of data-driven techniques to several societal and scientific fields and, of course, computational materials science has not been immuned to it. Therefore, at the present state, it seems that the development of future force fields will be based on such techniques.

The idea of implementing machine learning methods in molecular dynamics simulations derives from the necessity of performing simulations with *ab initio* accuracy, but at the cost of a classical simulation.

In this respect, ML methods are emerging as indispensable tools for 1) efficient and autonomous parameterization of FFs with known or pre-defined functional forms, and 2) directly learning the FF functional from the available high-fidelity AIMD and establishing a configuration-to-energy or force mapping.

The first approach has been already mentioned at the end of the previous section and consists in the parameterization (optimization of the parameters) of a simple functional form exploiting machine learning algorithms. One of the first examples of this approach in computational glass science has been provided by Liu et al. [212], who in 2019, optimized a simple 2-body interaction Buckingham potential for vitreous silica exploiting Gaussian Process Regression (GPR) [210,211] and the Bayesian Optimization (BO) approach [209,210]. In 2021, Christensen et al. [214] exploited the Particle Swarm Optimization (PSO) [215] algorithm to parameterize the same simple force field used by Liu et al. for vitreous silica. PSO is a stochastic population-based optimization method that mimics the behavior of bird flocking and that does not need gradient information. The PSO and GPR-BO FFs were observed to perform similarly. A different approach has been used by Yeon et al. [185], again in 2021, to develop an Mg/Al/Si/O reactive force field for magnesium aluminosilicate glasses. They exploited a Genetic Algorithm (GA) [216], coupled with an Artificial Neural Network (ANN) [217,218]. The GA mixes initial random parameters to obtain a new generation from which the best parameter's set is used to continue the dynasty and form a new generation. The ANN reads the GA results and improves the efficiency lowering the computational cost of the heuristic research by predicting the parameters and passing them to the GA. This

approach is proven to speed up the fitting of the parameters. Yeon et al. stated that 6 days were needed to train their FF on 500 CPUs.

Albeit, MD simulations with pre-defined functional forms continue to remain attractive owing to their 1) computational efficiency and 2) physical basis which imparts predictability and transferability for such models the poor flexibility in the simple functional form is one of the critical challenges which prevent their parameterization against large datasets of forces on atoms or energy at diverse configurations of the systems.

A more challenging application of ML algorithms is to predict directly energy and/or forces by exploiting their large flexibility. A schematic and generic flowchart of the supervised approach employed to devise i) Machine Learning (ML-) Potentials [219] and/or ii) Machine Learning FFs [220] is reported in Fig. 7. The general scheme is similar and it is composed of several steps: 1) generation of the QM dataset; 2) fingerprinting or featurization in which the atomic environment is encoded in numerical descriptors with proper physical and mathematical properties (permutational, rotational, and translational invariance); 3) training of the ML model and 4) validation of the model against unseen data. A deep description of these steps is reported in the recent reviews by Unke et al. [221] and Behler. [219].

The choice and optimization of the descriptors are crucial steps in the generation of a ML potential or FF. They encode the local environment of the atoms, within a predefined cutoff, into numerical vectors that can be read by the ML algorithm. The direct employment of the atomic coordinates is not possible because they are not invariant with respect to permutation, rotation, and translation. The easiest way to comply with these mathematical rules (that derive from the invariance of the energy with respect to these symmetrical operations) is to set a local framework on each atom and use the local coordinates of the neighbors. [222,223] These descriptors have the advantage of preserving all neighbor information, but they show an intrinsic non-smoothness as the continuous change in atom positions can give a discontinuous change of the atom numbering, the local frame, and consequently the local coordinates. [224] Often, the local environment (local coordinates) is embedded into more complex vectors or matrices using radial and/or angular expansion to generate smooth descriptors. [224,225] They allow maintaining the neighbor information introducing smoothness. This comes at the price of

more complex (and therefore computational expensive) descriptors. Examples of smooth descriptors are the symmetry functions from Behler and Parrinello (BPSF) [226,227] or the Smooth Overlap of Atomic Positions (SOAP) from Bartok et al. [228,229]

We specify that the nomenclature ML-potentials is usually used to refer to models that learn and predict the total energy of the entire system and consider the force calculations as secondary to energy calculations. [222,223,225,226,230,231] The total energy of the system is assumed to be composed of additive atomic contributions which are mapped through high-dimensional neural networks using atomic-centered structural descriptors (Atomic Centered Symmetry Functions, ACSF, as BPSF, [226,227] SOAP, [229,228] Coulomb Matrix (CM) [232], etc) computed with a certain cutoff. This approach allows to preserve the extensibility of the total energy and is based on the assumption that the energy of an atom only depends on its atomic coordinate and local environment. The latter assumption is clearly an approximation of the more complex nature of atomic interactions defining the system's energy which does not take into account non-local and non-additive terms. In particular, long-term effects (mainly deriving from Coulomb interactions) can be present and causes deviation from the local dependence assumption. For homogenous materials, these effects rapidly decrease when increasing the atomic distance and a sufficiently large cutoff allows satisfying the assumption. [224] Different methods have been proposed to handle the long-range interactions, [233–237] but there is still a lack of a widely accepted technique.

Instead, the nomenclature ML-FFs (Neural Networks or Kernel Ridge Regressions) is used for those models that directly predict the atomic forces by using vector structural descriptors as fingerprints of the atomic environments. The advantage of using the second approach is that the forces are true QM observables within the Born-Oppenheimer approximation, they can be calculated analytically at a low additional cost and a single calculation provides $3N$ (N = number of atoms) QM observables (forces) instead of a single one (total energy). However, it is worth noting that nowadays several codes like DeepMD [223] employ the partitioning of the energy in atomic contributions but including also the forces in the training sets beyond energy. Another benefit of a direct reconstruction of the forces is that it avoids the amplification of error

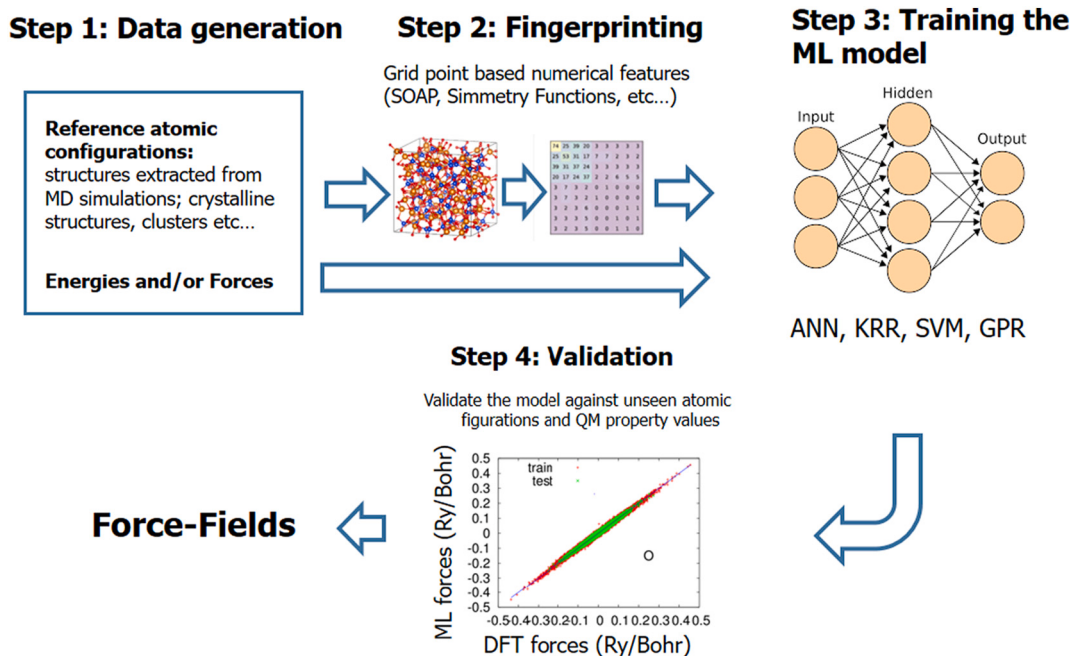


Fig. 7. Schematic representation of the supervised learning flowchart to generate ML interatomic potentials or ML Force-Fields. (ANN: Artificial Neural Networks, KRR: Kernel Ridge Regression, SVM: Support Vector Machine, GPR: Gaussian Process Regression).

estimations due to the application of the derivative operator but as a consequence energy conservation is not guaranteed, leading to the impossibility of running simulations in the micro-canonical ensemble (NVE).

The development of reliable ML-FFs or potentials hides several difficulties that have to be overcome. Firstly, the robustness of the ML models is strongly dependent on the number of diverse atomic configurations used in the training set and thus proper care must be devoted to widely exploring the PES of the system of interest. Enhanced sampling techniques and high temperatures AIMD simulations are usually used to generate a robust dataset for molecular systems or monocomponent solids. The development of transferrable FFs for multicomponent oxide glasses is also hampered by the enormous dimensionality of the compositional space since an infinite number of glass compositions can be generated by mixing more than two oxides. Different structural features are present depending on the glass composition. For example, Fig. 8 shows that adding Na_2O in silica glass leads to quite different Q^n distributions suggesting that ML-FFs or potentials trained on a silicate glass with a low amount of Na_2O where only Q^4 and Q^3 species are present will probably not be transferable to silicate glasses with high content of sodium oxide dominated by Q^1 and Q^0 species. The situation becomes even more complex for glasses with mixed network formers and/or modifiers.

ML techniques are inherently non-extrapolative methods and thus if during MD simulations the system explores configurations on which it has not been trained unpredictable results are produced. Therefore, clustering techniques should be used during MD simulations to measure the similarity of the instantaneous configuration with respect to those used during the training of the model and eventually re-train it on the fly. [238] Secondly, the transferability of the model to multicomponent systems requires the employment and optimization of weighted ACSFs [239] instead of the conventional ACSFs which describe different combinations of elements using separate functions and thus leading to a combinatorial explosion (the size of each atomic descriptor scales as $n(n+1)$ where n is the number of atomic species). New approaches, like the application of graph or convolutional neural networks, can overcome this limitation and further efforts are needed to facilitate the extension of the fitted potentials to new systems [240–243].

Albeit these approaches have been mainly examined to predict energy and forces for organic molecules [240,242,244] they are being increasingly used in the last few years also to accelerate MD simulations

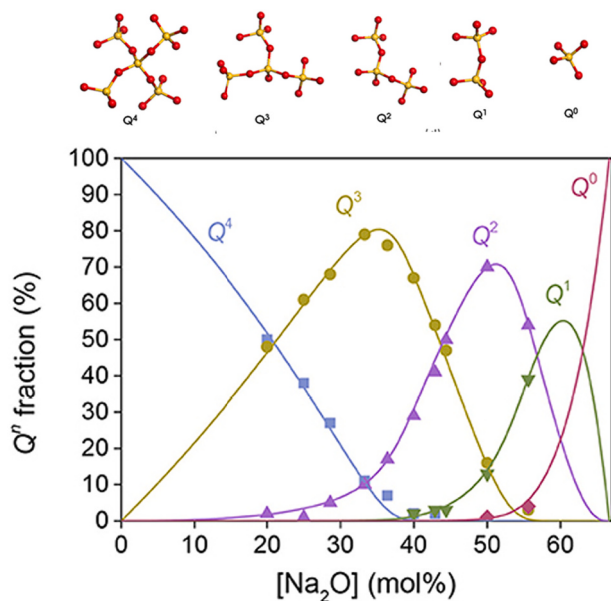


Fig. 8. Q^n distributions as a function of Na_2O content in sodium silicate glasses.

of oxide glasses. In 2020, Balyakin et al. [245] developed a neural network potential (NNP) for liquid silica using the DeepPot-SE [225] package implemented into the DeepMD [223] code. They trained a feedforward neural network [246] using more than 2,000,000 *ab initio* structures containing 96 atoms at different temperatures, obtaining a very good reproduction of the structure and dynamical properties of liquid silica. In 2022, Urata et al. [247] developed a NNP for silica, borosilicate glasses without modifiers, and fluorine-doped borosilicate glasses. They obtained good results in structure reproduction, even if undesired artifacts were observed at high temperatures during the dynamics. Again in 2022, Erhard et al. [248] used the Gaussian Approximation Potential (GAP) [231] framework to train a ML-potential for silica. They added in the training set liquid, glassy, and crystalline SiO_2 structures and some Si and O isolated dimers and clusters. Even if the simulations are very slower with respect to classical force fields, they can well reproduce amorphous and crystalline properties such as density (even at different pressure), X-ray diffraction pattern, phonon dispersion of α -quartz, and phase diagram but they lack in the reproduction of the medium range order of amorphous silica. In the same year, Batzner et al. [242] trained graph neural network [249] based interatomic potentials for various systems, including amorphous $\text{Li}_4\text{P}_2\text{O}_7$, a promising material for lithium transport in lithium-ion batteries [250], obtaining a very good prediction of forces, energies, and structural data.

Concerning the ML-FF, in 2018 Li and Ando [251] constructed linear, NN, and mixture [252] models for the prediction of forces in amorphous SiO_2 improving the prediction of the ring statics and vibrational density of states shown in Fig. 9.

In 2019, Mailoa et al. [253] trained a neural network for direct covariant force (DCF) prediction obtaining good results on amorphous $\text{Li}_4\text{P}_2\text{O}_7$. More recently, in 2021, Park et al. [241] trained a graph neural network to reproduce the forces on atoms in the same material (and Al_2O_3 -HF system) outperforming the DCF.

5. Final remarks

In this review, we have retraced the development of interatomic potentials for oxide glasses from the earlier investigations to the latest developments and applications. From this discussion and the number of works found in the literature, it is clear that the classical interatomic potentials based on the rigid ionic model with simple functional forms

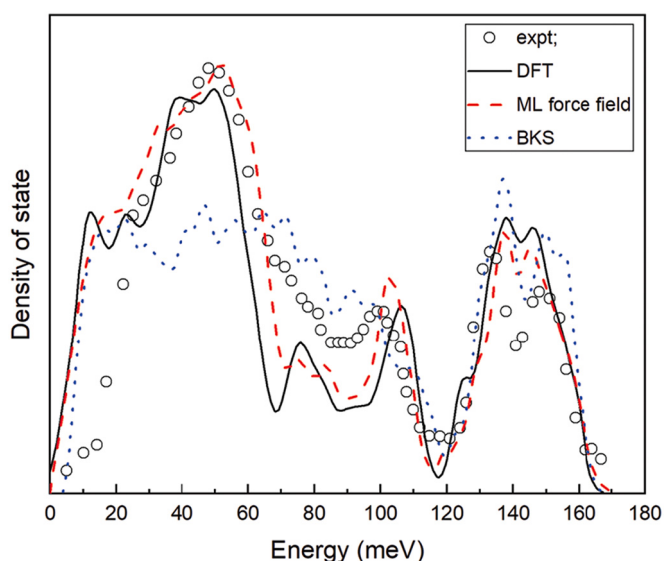


Fig. 9. Vibrational Density of States of SiO_2 glass computed with DFT (black curve), ML-FF (red dashed curve), and BKS potential (blue dot curve). The picture was taken from ref. [251]. (For interpretation of the references to colour in this figure legend, the reader is referred to the web version of this article.)

still dominate. They are the most used potentials for oxide glasses and they will continue to be the most applied for several reasons. Being usually composed of simple physics-based functional forms with a few parameters, they require fewer reference data and they are more easily parametrized with respect to the other models (polarizable and reactive FFs) and more efficient and easily transferable to compositions for which they have not been directly trained. Indeed, the libraries provided by Du's and Pedone's groups can cover a wide range of elements of the periodic table showing good transferability and accuracy allowing the self-consistent simulation of oxide glasses on a wide range of compositional space. On the contrary, the limited flexibility of the functional forms does not allow them to reproduce all the phase space of the system but only the low temperature structures. For the same reason, they are not trained against forces or energies but rather on structures and properties near the minima of interest and they are not suitable for the simulations of reactions.

Reactive force fields and ML-FFs are mandatory in these cases but their development and application is still limited. Much effort should be devoted to their extension to multicomponent oxide glasses since the actual applications were focused only on simple one or two component systems.

ML-FFs/potentials allow to simulate chemical-physical properties of molecules and condensed phases with QM accuracy in a fraction of the computational time required by high-level calculations but they are still 2–3 orders of magnitude more costly than empirical FFs (this is mainly due to the fingerprinting step) and they are not extrapolative techniques (since there is no physics in the model) and thus they are applicable to only the system for which they have been trained. Finally, the accuracy depends on the quality and dimension of the dataset used in training. This is a very time-consuming step and it is improbable that one research group alone will develop a transferable ML-FFs covering a wide compositional space as the rigid ionic potentials discussed above. Therefore, we think that a worldwide cooperative effort should be devoted to the generation of consistent quantum mechanical datasets. That is, a standard theoretical level (DFT functionals, pseudopotentials, etc) and procedure should be defined for simulating multicomponent oxide and non-oxide glasses. However, we are aware that this will be probably difficult to pursue also because of the continuous developments and improvements of the quantum mechanical methods.

Declaration of Competing Interest

The authors declare no conflict of interest that could have appeared to influence the work reported in this paper.

References

- [1] L.V. Woodcock, C.A. Angell, P. Cheeseman, Molecular dynamics studies of the vitreous state: Simple ionic systems and silica, *J. Chem. Phys.* 65 (1976) 1565–1577, <https://doi.org/10.1063/1.433213>.
- [2] R. Iftimie, P. Minary, M.E. Tuckerman, Ab initio molecular dynamics: Concepts, recent developments, and future trends, *Proc. Natl. Acad. Sci.* 102 (2005) 6654–6659, <https://doi.org/10.1073/pnas.0500193102>.
- [3] T.F. Soules, Molecular dynamic calculations of glass structure and diffusion in glass, *J. Non-Cryst. Solids* 49 (1982) 29–52, [https://doi.org/10.1016/0022-3093\(82\)90107-7](https://doi.org/10.1016/0022-3093(82)90107-7).
- [4] T.F. Soules, A molecular dynamic calculation of the structure of sodium silicate glasses, *J. Chem. Phys.* 71 (1979) 4570–4578, <https://doi.org/10.1063/1.438210>.
- [5] T.F. Soules, A.K. Varshneya, Molecular dynamic calculations of a sodium borosilicate glass structure, *J. Am. Ceram. Soc.* 64 (1981) 145–150, <https://doi.org/10.1111/j.1151-2916.1981.tb10246.x>.
- [6] S.K. Mitra, Molecular dynamics simulation of silicon dioxide glass, *Philos. Mag. B* 45 (1982) 529–548, <https://doi.org/10.1080/13642818208246417>.
- [7] S.K. Mitra, R.W. Hockney, Molecular dynamics simulation of the structure of soda silica, *Philos. Mag. B* 48 (1983) 151–167, <https://doi.org/10.1080/13642818308226467>.
- [8] S.H. Garofalini, A molecular dynamics simulation of the vitreous silica surface, *J. Chem. Phys.* 78 (1983) 2069–2072, <https://doi.org/10.1063/1.444927>.
- [9] S.H. Garofalini, S.M. Levine, Differences in surface behavior of Alkali ions in Li₂O · 3SiO₂ and Na₂O · 3SiO₂ glasses, *J. Am. Ceram. Soc.* 68 (1985) 376–379, <https://doi.org/10.1111/j.1151-2916.1985.tb10146.x>.
- [10] W.H. Zachariasen, The atomic arrangement in glass, *J. Am. Chem. Soc.* 54 (1932) 3841–3851, <https://doi.org/10.1021/ja01349a006>.
- [11] W. Soppe, C. van der Marel, W.F. van Gunsteren, H.W. den Hartog, New insights into the structure of B2O3 glass, *J. Non-Cryst. Solids* 103 (1988) 201–209, [https://doi.org/10.1016/0022-3093\(88\)90199-8](https://doi.org/10.1016/0022-3093(88)90199-8).
- [12] W. Soppe, H.W. den Hartog, A molecular dynamics study of (B2O3)_{1-x}–y(Li₂O)_x(Li₂Cl₂)_y and (B2O3)_{1-x}–y(Li₂O)(Cs₂O)_y, *J. Non-Cryst. Solids* 108 (1989) 260–268, [https://doi.org/10.1016/0022-3093\(89\)90296-2](https://doi.org/10.1016/0022-3093(89)90296-2).
- [13] J. Goubeau, H. Keller, RAMAN-Spektren und Struktur von Boroxol-Verbindungen, *Z. Für Anorg. Allg. Chem.* 272 (1953) 303–312, <https://doi.org/10.1002/zaac.19532720510>.
- [14] P.A.V. Johnson, A.C. Wright, R.N. Sinclair, A neutron diffraction investigation of the structure of vitreous boron trioxide, *J. Non-Cryst. Solids* 50 (1982) 281–311, [https://doi.org/10.1016/0022-3093\(82\)90092-8](https://doi.org/10.1016/0022-3093(82)90092-8).
- [15] G.E. Jellison, L.W. Panek, P.J. Bray, G.B. Rouse, Determinations of structure and bonding in vitreous B2O3 by means of B11, B11, and O17 NMR, *J. Chem. Phys.* 66 (1977) 802–812, <https://doi.org/10.1063/1.433959>.
- [16] B.P. Feuston, S.H. Garofalini, Empirical three-body potential for vitreous silica, *J. Chem. Phys.* 89 (1988) 5818–5824, <https://doi.org/10.1063/1.455531>.
- [17] R.G. Newell, B.P. Feuston, S.H. Garofalini, The structure of sodium trisilicate glass via molecular dynamics employing three-body potentials, *J. Mater. Res.* 4 (1989) 434–439, <https://doi.org/10.1557/JMR.1989.0434>.
- [18] M.J. Sanders, M. Leslie, C.R.A. Catlow, Interatomic potentials for SiO₂, *J. Chem. Soc. Chem. Commun.* (1984) 1271–1273, <https://doi.org/10.1039/C39840001271>.
- [19] B. Vessal, M. Amini, D. Fincham, C.R.A. Catlow, Water-like melting behaviour of SiO₂ investigated by the molecular dynamics simulation technique, *Philos. Mag. B* 60 (1989) 753–775, <https://doi.org/10.1080/13642818908209741>.
- [20] P. Vashishta, R.K. Kalia, J.P. Rino, I. Ebbsjö, Interaction potential for \$[\mathrm{SiO}_4]_2\$: A molecular-dynamics study of structural correlations, *Phys. Rev. B* 41 (1990) 12197–12209, <https://doi.org/10.1103/PhysRevB.41.12197>.
- [21] G.V. Lewis, C.R.A. Catlow, Potential models for ionic oxides, *J. Phys. C Solid State Phys.* 18 (1985) 1149–1161, <https://doi.org/10.1088/0022-3719/18/6/010>.
- [22] S.C. Parker, C.R.A. Catlow, A.N. Cormack, Structure prediction of silicate minerals using energy-minimization techniques, *Acta Crystallogr. B* 40 (1984) 200–208, <https://doi.org/10.1107/S0108768184001981>.
- [23] C. Huang, A.N. Cormack, The structure of sodium silicate glass, *J. Chem. Phys.* 93 (1990) 8180–8186, <https://doi.org/10.1063/1.459296>.
- [24] C. Huang, A.N. Cormack, Structural differences and phase separation in alkali silicate glasses, *J. Chem. Phys.* 95 (1991) 3634–3642, <https://doi.org/10.1063/1.460814>.
- [25] C. Huang, A.N. Cormack, Structure and energetics in mixed-alkali-metal silicate glasses from molecular dynamics, *J. Mater. Chem.* 2 (1992) 281–287, <https://doi.org/10.1039/JM9920200281>.
- [26] W. Smith, G.N. Greaves, M.J. Gillan, Computer simulation of sodium disilicate glass, *J. Chem. Phys.* 103 (1995) 3091–3097, <https://doi.org/10.1063/1.470498>.
- [27] W. Smith, T.R. Forester, G. Neville Greaves, S. Hayter, M.J. Gillan, Molecular dynamics simulation of alkali-metal diffusion in alkali-metal disilicate glasses, *J. Mater. Chem.* 7 (1997) 331–336, <https://doi.org/10.1039/A606185K>.
- [28] G.N. Greaves, Structural studies of the mixed alkali effect in disilicate glasses, *Solid State Ionics* 105 (1998) 243–248, [https://doi.org/10.1016/S0167-2738\(97\)00471-2](https://doi.org/10.1016/S0167-2738(97)00471-2).
- [29] H. Melman, S.H. Garofalini, Microstructural evaluation of simulated sodium silicate glasses, *J. Non-Cryst. Solids* 134 (1991) 107–115, [https://doi.org/10.1016/0022-3093\(91\)90017-Z](https://doi.org/10.1016/0022-3093(91)90017-Z).
- [30] B. Vessal, G.N. Greaves, P.T. Marten, A.V. Chadwick, R. Mole, S. Houde-Walter, Cation microsegregation and ionic mobility in mixed alkali glasses, *Nature*. 356 (1992) 504–506, <https://doi.org/10.1038/356504a0>.
- [31] S. Balasubramanian, K.J. Rao, A molecular dynamics study of the mixed alkali effect in silicate glasses, *J. Non-Cryst. Solids* 181 (1995) 157–174, [https://doi.org/10.1016/0022-3093\(94\)00489-7](https://doi.org/10.1016/0022-3093(94)00489-7).
- [32] G.N. Greaves, A. Fontaine, P. Lagarde, D. Raoux, S.J. Gurman, Local structure of silicate glasses, *Nature*. 293 (1981) 611–616, <https://doi.org/10.1038/293611a0>.
- [33] G.N. Greaves, EXAFS and the structure of glass, *J. Non-Cryst. Solids* 71 (1985) 203–217, [https://doi.org/10.1016/0022-3093\(85\)90289-3](https://doi.org/10.1016/0022-3093(85)90289-3).
- [34] A.N. Cormack, Y. Cao, Molecular dynamics simulation of silicate glasses, *Mol. Eng.* 6 (1996) 183–227, <https://doi.org/10.1007/BF00161727>.
- [35] Y. Onodera, Y. Takimoto, H. Hijiya, T. Taniguchi, S. Urata, S. Inaba, S. Fujita, I. Obayashi, Y. Hiraoka, S. Kohara, Origin of the mixed alkali effect in silicate glass, *NPG Asia Mater.* 11 (2019) 1–11, <https://doi.org/10.1038/s41427-019-0180-4>.
- [36] K. Hirao, N. Soga, Molecular dynamic simulation of Eu³⁺-doped sodium borate glasses and their fluorescence spectra, *J. Am. Ceram. Soc.* 68 (1985) 515–521, <https://doi.org/10.1111/j.1151-2916.1985.tb11516.x>.
- [37] H. Inoue, N. Aoki, I. Yasui, Molecular dynamics simulation of the structure of borate glasses, *J. Am. Ceram. Soc.* 70 (1987) 622–627, <https://doi.org/10.1111/j.1151-2916.1987.tb05729.x>.
- [38] A. Takada, C.R.A. Catlow, G.D. Price, Computer modelling of B2O3. II. Molecular dynamics simulations of vitreous structures, *J. Phys. Condens. Matter* 7 (1995) 8693–8722, <https://doi.org/10.1088/0953-8984/7/46/004>.
- [39] B. Park, A.N. Cormack, Molecular dynamics simulation of Alkali borate glass using coordination dependent potential, *MRS Online Proc. Libr. OPL*. 455 (1996), <https://doi.org/10.1557/PROC-455-259>.
- [40] A.N. Cormack, B. Park, Molecular dynamics simulations of borate glasses, *Phys. Chem. Glasses* 41 (2000) 272–277.

- [41] S. Tsuneyuki, M. Tsukada, H. Aoki, Y. Matsui, First-principles interatomic potential of silica applied to molecular dynamics, Phys. Rev. Lett. 61 (1988) 869–872, <https://doi.org/10.1103/PhysRevLett.61.869>.
- [42] B.W.H. van Beest, G.J. Kramer, R.A. van Santen, Force fields for silicas and aluminophosphates based on ab initio calculations, Phys. Rev. Lett. 64 (1990) 1955–1958, <https://doi.org/10.1103/PhysRevLett.64.1955>.
- [43] J.R. Chelikowsky, H.E. King, N. Troullier, J. Lus Martins, J. Glinnemann, Structural properties of α -quartz near the amorphous transition, Phys. Rev. Lett. 65 (1990) 3309–3312, <https://doi.org/10.1103/PhysRevLett.65.3309>.
- [44] R.G. Della Valle, H.C. Andersen, Test of a pairwise additive ionic potential model for silica, J. Chem. Phys. 94 (1991) 5056–5060, <https://doi.org/10.1063/1.460541>.
- [45] R.G. Della Valle, E. Venuti, A molecular dynamics study of the vibrational properties of silica glass, Chem. Phys. 179 (1994) 411–419, [https://doi.org/10.1016/0301-0104\(94\)87017-9](https://doi.org/10.1016/0301-0104(94)87017-9).
- [46] R.G. Della Valle, E. Venuti, High-pressure densification of silica glass: A molecular-dynamics simulation, Phys. Rev. B 54 (1996) 3809–3816, <https://doi.org/10.1103/PhysRevB.54.3809>.
- [47] D. Herzbach, K. Binder, M.H. Müser, Comparison of model potentials for molecular-dynamics simulations of silica, J. Chem. Phys. 123 (2005), 124711, <https://doi.org/10.1063/1.2038747>.
- [48] I. Saika-Voivod, P.H. Poole, F. Sciotino, Fragile-to-strong transition and polyamorphism in the energy landscape of liquid silica, Nature. 412 (2001) 514–517, <https://doi.org/10.1038/35087524>.
- [49] T.F. Soules, G.H. Gilmer, M.J. Matthews, J.S. Stolken, M.D. Feit, Silica molecular dynamic force fields—A practical assessment, J. Non-Cryst. Solids 357 (2011) 1564–1573, <https://doi.org/10.1016/j.jnoncrysol.2011.01.009>.
- [50] J.S. Tse, D.D. Klug, The structure and dynamics of silica polymorphs using a two-body effective potential model, J. Chem. Phys. 95 (1991) 9176–9185, <https://doi.org/10.1063/1.461198>.
- [51] J.S. Tse, D.D. Klug, Y. Le Page, High-pressure densification of amorphous silica, Phys. Rev. B 46 (1992) 5933–5938, <https://doi.org/10.1103/PhysRevB.46.5933>.
- [52] K. Vollmayr, W. Kob, K. Binder, Cooling-rate effects in amorphous silica: A computer-simulation study, Phys. Rev. B 54 (1996) 15808–15827, <https://doi.org/10.1103/PhysRevB.54.15808>.
- [53] G. Malavasi, M.C. Menziani, A. Pedone, U. Segre, Void size distribution in MD-modelled silica glass structures, J. Non-Cryst. Solids 352 (2006) 285–296, <https://doi.org/10.1016/j.jnoncrysol.2005.11.022>.
- [54] F. Yuan, L. Huang, Molecular dynamics simulation of amorphous silica under uniaxial tension: From bulk to nanowire, J. Non-Cryst. Solids 358 (2012) 3481–3487, <https://doi.org/10.1016/j.jnoncrysol.2012.05.045>.
- [55] M. Hemmati, C. Austen Angell, IR absorption of silicate glasses studied by ion dynamics computer simulation. I. IR spectra of SiO₂ glass in the rigid ion model approximation, J. Non-Cryst. Solids 217 (1997) 236–249, [https://doi.org/10.1016/S0022-3093\(97\)00135-X](https://doi.org/10.1016/S0022-3093(97)00135-X).
- [56] L. Huang, J. Kieffer, Challenges in modeling mixed ionic-covalent glass formers, in: C. Massobrio, J. Du, M. Bernasconi, P.S. Salmon (Eds.), Mol. Dyn. Simul. Disord. Mater. Netw. Glas. Phase-Change Mem. Alloys, Springer International Publishing, Cham, 2015, pp. 87–112, https://doi.org/10.1007/978-3-319-15675-0_4.
- [57] A. Pedone, G. Malavasi, M.C. Menziani, U. Segre, F. Musso, M. Corno, B. Civalleri, P. Ugliengo, FFSiOH: a new force field for silica polymorphs and their hydroxylated surfaces based on periodic B3LYP calculations, Chem. Mater. 20 (2008) 2522–2531, <https://doi.org/10.1021/cm703437y>.
- [58] P. Tangney, S. Scandolo, An ab initio parametrized interatomic force field for silica, J. Chem. Phys. 117 (2002) 8898–8904, <https://doi.org/10.1063/1.1513312>.
- [59] J. Habasaki, Molecular-dynamics study of glass formation in the Li₂SiO₃ system, Mol. Phys. (2006), <https://doi.org/10.1080/0026897900101161>.
- [60] J. Habasaki, I. Okada, Molecular dynamics simulation of Alkali silicates based on the quantum mechanical potential surfaces, Mol. Simul. 9 (1992) 319–326, <https://doi.org/10.1080/08927029208049124>.
- [61] J. Habasaki, I. Okada, Y. Hiwatari, Glass transition temperatures studied by MD simulation of some Alkali metasilicates, Mol. Simul. 10 (1993) 19–26, <https://doi.org/10.1080/08927029308022495>.
- [62] R.D. Banhatti, A. Heuer, Structure and dynamics of lithium silicate melts: molecular dynamics simulations, Phys. Chem. Chem. Phys. 3 (2001) 5104–5108, <https://doi.org/10.1039/B106013A>.
- [63] A. Heuer, M. Kunow, M. Vogel, R.D. Banhatti, Characterization of the complex ion dynamics in lithium silicate glasses via computer simulations, Phys. Chem. Chem. Phys. 4 (2002) 3185–3192, <https://doi.org/10.1039/B201121B>.
- [64] H. Lamertz, M. Kunow, A. Heuer, Complete identification of Alkali sites in ion conducting lithium silicate glasses: a computer study of ion dynamics, Phys. Rev. Lett. 90 (2003), 215901, <https://doi.org/10.1103/PhysRevLett.90.215901>.
- [65] J. Horbach, W. Kob, K. Binder, Dynamics of sodium in sodium disilicate: channel relaxation and sodium diffusion, Phys. Rev. Lett. 88 (2002), 125502, <https://doi.org/10.1103/PhysRevLett.88.125502>.
- [66] P. Jund, W. Kob, R. Jullien, Channel diffusion of sodium in a silicate glass, Phys. Rev. B 64 (2001), 134303, <https://doi.org/10.1103/PhysRevB.64.134303>.
- [67] X. Yuan, A.N. Cormack, Local structures of MD-modeled vitreous silica and sodium silicate glasses, J. Non-Cryst. Solids 283 (2001) 69–87, [https://doi.org/10.1016/S0022-3093\(01\)00363-5](https://doi.org/10.1016/S0022-3093(01)00363-5).
- [68] A.N. Cormack, J. Du, T.R. Zeitler, Sodium ion migration mechanisms in silicate glasses probed by molecular dynamics simulations, J. Non-Cryst. Solids 323 (2003) 147–154, [https://doi.org/10.1016/S0022-3093\(03\)00280-1](https://doi.org/10.1016/S0022-3093(03)00280-1).
- [69] J. Du, A.N. Cormack, The medium range structure of sodium silicate glasses: a molecular dynamics simulation, J. Non-Cryst. Solids 349 (2004) 66–79, <https://doi.org/10.1016/j.jnoncrysol.2004.08.264>.
- [70] J. Du, A.N. Cormack, Molecular dynamics simulation of the structure and hydroxylation of silica glass surfaces, J. Am. Ceram. Soc. 88 (2005) 2532–2539, <https://doi.org/10.1111/j.1551-2916.2005.00352.x>.
- [71] J. Du, A.N. Cormack, The structure of erbium doped sodium silicate glasses, J. Non-Cryst. Solids 351 (2005) 2263–2276, <https://doi.org/10.1016/j.jnoncrysol.2005.05.018>.
- [72] J. Du, L.R. Corrales, Compositional dependence of the first sharp diffraction peaks in alkali silicate glasses: A molecular dynamics study, J. Non-Cryst. Solids 352 (2006) 3255–3269, <https://doi.org/10.1016/j.jnoncrysol.2006.05.025>.
- [73] J. Du, L. René Corrales, Understanding lanthanum aluminate glass structure by correlating molecular dynamics simulation results with neutron and X-ray scattering data, J. Non-Cryst. Solids 353 (2007) 210–214, <https://doi.org/10.1016/j.jnoncrysol.2006.06.025>.
- [74] J. Du, Molecular dynamics simulations of the structure and properties of low silica yttrium aluminosilicate glasses, J. Am. Ceram. Soc. 92 (2009) 87–95, <https://doi.org/10.1111/j.1551-2916.2008.02853.x>.
- [75] J. Du, L. Kokou, Europium environment and clustering in europium doped silica and sodium silicate glasses, J. Non-Cryst. Solids 357 (2011) 2235–2240, <https://doi.org/10.1016/j.jnoncrysol.2010.11.088>.
- [76] J. Du, L. Kokou, J.L. Rygel, Y. Chen, C.G. Pantano, R. Woodman, J. Belcher, Structure of cerium phosphate glasses: molecular dynamics simulation, J. Am. Ceram. Soc. 94 (2011) 2393–2401, <https://doi.org/10.1111/j.1551-2916.2011.04514.x>.
- [77] J. Du, Y. Xiang, Effect of strontium substitution on the structure, ionic diffusion and dynamic properties of 4S5 Bioactive glasses, J. Non-Cryst. Solids 358 (2012) 1059–1071, <https://doi.org/10.1016/j.jnoncrysol.2011.12.114>.
- [78] J. Du, Challenges in molecular dynamics simulations of multicomponent oxide glasses, in: C. Massobrio, J. Du, M. Bernasconi, P.S. Salmon (Eds.), Mol. Dyn. Simul. Disord. Mater. Netw. Glas. Phase-Change Mem. Alloys, Springer International Publishing, Cham, 2015, pp. 157–180, https://doi.org/10.1007/978-3-319-15675-0_7.
- [79] L. Deng, J. Du, Development of boron oxide potentials for computer simulations of multicomponent oxide glasses, J. Am. Ceram. Soc. (2018) 1–24, <https://doi.org/10.1111/jace.16082>.
- [80] W.J. Dell, P.J. Bray, S.Z. Xiao, 11B NMR studies and structural modeling of Na₂₀B₂O₃ SiO₂ glasses of high soda content, J. Non-Cryst. Solids 58 (1983) 1–16, [https://doi.org/10.1016/0022-3093\(83\)90097-2](https://doi.org/10.1016/0022-3093(83)90097-2).
- [81] M.I. Tuheen, L. Deng, J. Du, A comparative study of the effectiveness of empirical potentials for molecular dynamics simulations of borosilicate glasses, J. Non-Cryst. Solids 553 (2021), 120413, <https://doi.org/10.1016/j.jnoncrysol.2020.120413>.
- [82] M. Fortino, A. Berselli, N. Stone-Weiss, L. Deng, A. Goel, J. Du, A. Pedone, Assessment of interatomic parameters for the reproduction of borosilicate glass structures via DFT-GIPAW calculations, J. Am. Ceram. Soc. 102 (2019) 7225–7243, <https://doi.org/10.1111/jace.16655>.
- [83] A. Pedone, G. Malavasi, M.C. Menziani, A.N. Cormack, U. Segre, A new self-consistent empirical interatomic potential model for oxides, silicates, and silica-based glasses, J. Phys. Chem. B 110 (2006) 11780–11795, <https://doi.org/10.1021/jp0611018>.
- [84] G. Ori, M. Montorsi, A. Pedone, C. Siligardi, Insight into the structure of vanadium containing glasses: A molecular dynamics study, J. Non-Cryst. Solids 357 (2011) 2571–2579, <https://doi.org/10.1016/j.jnoncrysol.2011.02.002>.
- [85] G. Malavasi, A. Pedone, M.C. Menziani, Study of the structural role of gallium and aluminum in 4S5 bioactive glasses by molecular dynamics simulations, J. Phys. Chem. B 117 (2013) 4142–4150, <https://doi.org/10.1021/jp400721g>.
- [86] A. Pedone, Properties calculations of silica-based glasses by atomistic simulations techniques: A review, J. Phys. Chem. C 113 (2009) 20773–20784, <https://doi.org/10.1021/jp9071263>.
- [87] A.A. Hassanali, S.J. Singer, Model for the water–amorphous silica interface: the undissociated surface, J. Phys. Chem. B 111 (2007) 11181–11193, <https://doi.org/10.1021/jp062971s>.
- [88] B.M. Al-Hasni, G. Mountjoy, A molecular dynamics study of the atomic structure of x(MgO) 100–x(SiO₂), J. Non-Cryst. Solids 400 (2014) 33–44, <https://doi.org/10.1016/j.jnoncrysol.2013.11.011>.
- [89] F. Angeli, O. Villain, S. Schuller, S. Ispas, T. Charpentier, Insight into sodium silicate glass structural organization by multinuclear NMR combined with first-principles calculations, Geochim. Cosmochim. Acta 75 (2011) 2453–2469, <https://doi.org/10.1016/j.gca.2011.02.003>.
- [90] Y. Deng, C. Eames, J.-N. Chotard, P. Lalère, V. Seznec, S. Emge, O. Pecher, C. P. Grey, C. Masquelier, M.S. Islam, Structural and mechanistic insights into fast lithium-ion conduction in Li₄SiO₄–Li₃PO₄ solid electrolytes, J. Am. Chem. Soc. 137 (2015) 9136–9145, <https://doi.org/10.1021/jacs.5b04444>.
- [91] M.E. McKenzie, S. Goyal, T. Loeffler, L. Cai, I. Dutta, D.E. Baker, J.C. Mauro, Implicit glass model for simulation of crystal nucleation for glass-ceramics, Npj Comput. Mater. 4 (2018) 1–7, <https://doi.org/10.1038/s41524-018-0116-5>.
- [92] L.B. Skinner, A.C. Barnes, P.S. Salmon, L. Hennet, H.E. Fischer, C.J. Benmore, S. Kohara, J.K.R. Weber, A. Bytchkov, M.C. Wilding, J.B. Parise, T.O. Farmer, I. Pozdnyakova, S.K. Tumber, K. Ohara, Joint diffraction and modeling approach to the structure of liquid alumina, Phys. Rev. B 87 (2013), 024201, <https://doi.org/10.1103/PhysRevB.87.024201>.
- [93] S. Urata, R. Ando, M. Ono, Y. Hayashi, Molecular dynamics study on nanoparticles reinforced oxide glass, J. Am. Ceram. Soc. 101 (2018) 2266–2276, <https://doi.org/10.1111/jace.15378>.

- [94] S.M. Wood, C. Eames, E. Kendrick, M.S. Islam, Sodium ion diffusion and voltage trends in phosphates Na4M3(PO4)2P2O7 (M = Fe, Mn, Co, Ni) for possible high-rate cathodes, *J. Phys. Chem. C* 119 (2015) 15935–15941, <https://doi.org/10.1021/acs.jpcc.5b04648>.
- [95] S. Urata, Y. Takato, K. Maeda, Molecular dynamics investigation of the fracture mechanism of a glass-ceramic containing cleavable crystals, *J. Am. Ceram. Soc.* 102 (2019) 5138–5148, <https://doi.org/10.1111/jace.16399>.
- [96] K. Konstantinou, P.V. Sushko, D.M. Duffy, Structure and ionic diffusion of alkaline-earth ions in mixed cation glasses A2O–2MO–4SiO2 with molecular dynamics simulations, *J. Non-Cryst. Solids* 422 (2015) 57–63, <https://doi.org/10.1016/j.jnoncrysol.2015.05.005>.
- [97] B. Guillot, N. Sator, A computer simulation study of natural silicate melts. Part I: Low pressure properties, *Geochim. Cosmochim. Acta* 71 (2007) 1249–1265, <https://doi.org/10.1016/j.gca.2006.11.015>.
- [98] M. Bauchy, B. Guillot, M. Micoulaut, N. Sator, Viscosity and viscosity anomalies of model silicates and magmas: A numerical investigation, *Chem. Geol.* 346 (2013) 47–56, <https://doi.org/10.1016/j.chemgeo.2012.08.035>.
- [99] B. Guillot, N. Sator, Carbon dioxide in silicate melts: A molecular dynamics simulation study, *Geochim. Cosmochim. Acta* 75 (2011) 1829–1857, <https://doi.org/10.1016/j.gca.2011.01.004>.
- [100] B. Guillot, N. Sator, A computer simulation study of natural silicate melts. Part II: High pressure properties, *Geochim. Cosmochim. Acta* 71 (2007) 4538–4556, <https://doi.org/10.1016/j.gca.2007.05.029>.
- [101] C. Siakati, R. Macchieraldo, B. Kirchner, F. Tielens, A. Peys, D. Seveno, Y. Pontikes, Unraveling the nano-structure of a glassy CaO–FeO–SiO2 slag by molecular dynamics simulations, *J. Non-Cryst. Solids* 528 (2020), 119771, <https://doi.org/10.1016/j.jnoncrysol.2019.119771>.
- [102] F. Lodesani, M.C. Menziani, H. Hijiya, Y. Takato, S. Urata, A. Pedone, Structural origins of the mixed alkali effect in alkali aluminosilicate glasses: molecular dynamics study and its assessment, *Sci. Rep.* 10 (2020) 1–18, <https://doi.org/10.1038/s41598-020-59875-7>.
- [103] L.-H. Kieu, J.-M. Delaye, L. Cormier, C. Stoltz, Development of empirical potentials for sodium borosilicate glass systems, *J. Non-Cryst. Solids* 357 (2011) 3313–3321, <https://doi.org/10.1016/j.jnoncrysol.2011.05.024>.
- [104] M. Wang, N.M. Anoop Krishnan, B. Wang, M.M. Smedskjaer, J.C. Mauro, M. Bauchy, A new transferable interatomic potential for molecular dynamics simulations of borosilicate glasses, *J. Non-Cryst. Solids* 498 (2018) 294–304, <https://doi.org/10.1016/j.jnoncrysol.2018.04.063>.
- [105] S. Sundararaman, L. Huang, S. Ispas, W. Kob, New optimization scheme to obtain interaction potentials for oxide glasses, *J. Chem. Phys.* 148 (2018), 194504, <https://doi.org/10.1063/1.5023707>.
- [106] S. Sundararaman, L. Huang, S. Ispas, W. Kob, New interaction potentials for alkali and alkaline-earth aluminosilicate glasses, *J. Chem. Phys.* 150 (2019), 154505, <https://doi.org/10.1063/1.5079663>.
- [107] S. Sundararaman, L. Huang, S. Ispas, W. Kob, New interaction potentials for borate glasses with mixed network formers, *J. Chem. Phys.* 152 (2020), 104501, <https://doi.org/10.1063/1.5142605>.
- [108] D. Wolf, P. Kebinski, S.R. Phillpot, J. Eggebrecht, Exact method for the simulation of Coulombic systems by spherically truncated, pairwise r–1 summation, *J. Chem. Phys.* 110 (1999) 8254–8282, <https://doi.org/10.1063/1.478738>.
- [109] Z. Zhang, S. Ispas, W. Kob, Origin of the non-linear elastic behavior of silicate glasses, *Acta Mater.* 231 (2022), 117855, <https://doi.org/10.1016/j.actamat.2022.117855>.
- [110] Z. Zhang, S. Ispas, W. Kob, The critical role of the interaction potential and simulation protocol for the structural and mechanical properties of sodosilicate glasses, *J. Non-Cryst. Solids* 532 (2020), 119895, <https://doi.org/10.1016/j.jnoncrysol.2020.119895>.
- [111] B.G. Dick, A.W. Overhauser, Theory of the dielectric constants of Alkali Halide crystals, *Phys. Rev.* 112 (1958) 90–103, <https://doi.org/10.1103/PhysRev.112.90>.
- [112] A. Pedone, T. Charpentier, G. Malavasi, M.C. Menziani, New insights into the atomic structure of 45SS bioglass by means of solid-state NMR spectroscopy and accurate first-principles simulations, *Chem. Mater.* 22 (2010) 5644–5652, <https://doi.org/10.1021/cm102089c>.
- [113] T. Charpentier, P. Kroll, F. Mauri, First-Principles Nuclear Magnetic Resonance Structural Analysis of Vitreous Silica, 2009, <https://doi.org/10.1021/jp900297r>.
- [114] T. Charpentier, M.C. Menziani, A. Pedone, Computational simulations of solid state NMR spectra: a new era in structure determination of oxide glasses, *RSC Adv.* 3 (2013) 10550–10578, <https://doi.org/10.1039/c3ra40627>.
- [115] A. Pedone, E. Gambuzzi, M.C. Menziani, Unambiguous description of the oxygen environment in multicomponent aluminosilicate glasses from O-17 solid state NMR computational spectroscopy, *J. Phys. Chem. C* 116 (2012) 14599–14609, <https://doi.org/10.1021/jp304802y>.
- [116] A. Pedone, E. Gambuzzi, G. Malavasi, M.C. Menziani, First-principles simulations of the Al-27 and O-17 solid-state NMR spectra of the CaAl2Si3O10 glass, *Theor. Chem. Accounts* 131 (2012) 1147, <https://doi.org/10.1007/s00214-012-1147-5>.
- [117] A. Pedone, T. Charpentier, M.C. Menziani, The structure of fluoride-containing bioactive glasses: new insights from first-principles calculations and solid state NMR spectroscopy, *J. Mater. Chem.* 22 (2012) 12599–12608, <https://doi.org/10.1039/c2jm30890h>.
- [118] A. Pedone, T. Charpentier, M.C. Menziani, Multinuclear NMR of CaSiO3 glass: simulation from first-principles, *Phys. Chem. Chem. Phys.* 12 (2010) 6054–6066, <https://doi.org/10.1039/b924489a>.
- [119] A. Pedone, Recent advances in solid-state NMR computational spectroscopy: the case of aluminosilicate glasses, *Int. J. Quantum Chem.* 116 (2016) 1520–1531, <https://doi.org/10.1002/qua.25134>.
- [120] E. Gambuzzi, A. Pedone, M.C. Menziani, F. Angeli, P. Florian, T. Charpentier, Calcium environment in silicate and aluminosilicate glasses probed by Ca-43 MQMAS NMR experiments and MD-GIPAW calculations, *Solid State Nucl. Magn. Reson.* 68–69 (2015) 31–36, <https://doi.org/10.1016/j.ssnmr.2015.04.003>.
- [121] S. Ispas, T. Charpentier, F. Mauri, D.R. Neuville, Structural properties of lithium and sodium tetrasilicate glasses: Molecular dynamics simulations versus NMR experimental and first-principles data, *Solid State Sci.* 12 (2010) 183–192, <https://doi.org/10.1016/j.jssolidstatesciences.2009.06.033>.
- [122] T.M. Clark, P.J. Grandinetti, P. Florian, J.F. Stebbins, Correlated structural distributions in silica glass, *Phys. Rev. B* 70 (2004), 064202, <https://doi.org/10.1103/PhysRevB.70.064202>.
- [123] T. Charpentier, K. Okhotnikov, A.N. Novikov, L. Hennet, H.E. Fischer, D. R. Neuville, P. Florian, Structure of strontium aluminosilicate glasses from molecular dynamics simulation, neutron diffraction, and nuclear magnetic resonance studies, *J. Phys. Chem. B* 122 (2018) 9567–9583, <https://doi.org/10.1021/acs.jpcb.8b05721>.
- [124] M. Bertani, M.C. Menziani, A. Pedone, Improved empirical force field for multicomponent oxide glasses and crystals, *Phys. Rev. Mater.* 5 (2021), 045602, <https://doi.org/10.1103/PhysRevMaterials.5.045602>.
- [125] B. Stevenson, Y. Yu, M. Edén, Structure–composition trends in multicomponent borosilicate-based glasses deduced from molecular dynamics simulations with improved B–O and P–O force fields, *Phys. Chem. Chem. Phys.* 20 (2018) 8192–8209, <https://doi.org/10.1039/C7CP08593A>.
- [126] M. Bertani, A. Pallini, M. Cocchi, M.C. Menziani, A. Pedone, A new self-consistent empirical potential model for multicomponent borate and borosilicate glasses, *J. Am. Ceram. Soc.* (2022), <https://doi.org/10.1111/jace.18681> n/a (n.d.).
- [127] C.R.A. Catlow, *Computer Modeling in Inorganic Crystallography*, Elsevier, 1997.
- [128] R.T. Cygan, J.D. Kubicki, *Molecular Modeling Theory: Applications in the Geosciences*, Walter de Gruyter GmbH & Co KG, 2018.
- [129] P.A. Madden, M. Wilson, ‘Covalent’ effects in ‘ionic’ systems, *Chem. Soc. Rev.* 25 (1996) 339–350, <https://doi.org/10.1039/CS962500339>.
- [130] A. Pedone, X. Chen, R.G. Hill, A. Karpukhina, Molecular dynamics investigation of Halide-containing Phospho-silicate bioactive glasses, *J. Phys. Chem. B* 122 (2018) 2940–2948, <https://doi.org/10.1021/acs.jpcb.8b00547>.
- [131] A. Tilocca, N.H. de Leeuw, A.N. Cormack, Shell-model molecular dynamics calculations of modified silicate glasses, *Phys. Rev. B* 73 (2006), 104209, <https://doi.org/10.1103/PhysRevB.73.104209>.
- [132] A. Tilocca, Structural models of bioactive glasses from molecular dynamics simulations, *Proc. R. Soc. Math. Phys. Eng. Sci.* 465 (2009) 1003–1027, <https://doi.org/10.1098/rspa.2008.0462>.
- [133] A. Tilocca, A.N. Cormack, Structural effects of phosphorus inclusion in bioactive silicate glasses, *J. Phys. Chem. B* 111 (2007) 14256–14264, <https://doi.org/10.1021/jp0756707>.
- [134] A. Tilocca, A.N. Cormack, N.H. de Leeuw, The structure of bioactive silicate glasses: new insight from molecular dynamics simulations, *Chem. Mater.* 19 (2007) 95–103, <https://doi.org/10.1021/cm061631g>.
- [135] A. Tilocca, Short- and medium-range structure of multicomponent bioactive glasses and melts: An assessment of the performances of shell-model and rigid-ion potentials, *J. Chem. Phys.* 129 (2008), 084504, <https://doi.org/10.1063/1.2972146>.
- [136] A. Pedone, G. Malavasi, M.C. Menziani, Computational insight into the effect of CaO/MgO substitution on the structural properties of phospho-silicate bioactive glasses, *J. Phys. Chem. C* 113 (2009) 15723–15730, <https://doi.org/10.1021/jp904131t>.
- [137] E. Gambuzzi, A. Pedone, On the structure of Ce-containing silicophosphate glasses: a core-shell molecular dynamics investigation, *Phys. Chem. Chem. Phys.* 16 (2014) 21645–21656, <https://doi.org/10.1039/c4cp02577f>.
- [138] V. Nicolini, E. Gambuzzi, G. Malavasi, L. Menabue, M.C. Menziani, G. Lusvardi, A. Pedone, F. Benedetti, P. Luches, S. D’Addato, S. Valeri, Evidence of catalase mimetic activity in Ce3+/Ce4+ doped bioactive glasses, *J. Phys. Chem. B* 119 (2015) 4009–4019, <https://doi.org/10.1021/jp511737b>.
- [139] A. Pedone, F. Muniz-Miranda, A. Tilocca, M.C. Menziani, The antioxidant properties of Ce-containing bioactive glass nanoparticles explained by molecular dynamics simulations, *Biomed. Glas.* 1 (2016), <https://doi.org/10.1515/bglass-2016-0003>.
- [140] E. Gambuzzi, A. Pedone, M.C. Menziani, F. Angeli, D. Caurant, T. Charpentier, Probing silicon and aluminium chemical environments in silicate and aluminosilicate glasses by solid state NMR spectroscopy and accurate first-principles calculations, *Geochim. Cosmochim. Acta* 125 (2014) 170–185, <https://doi.org/10.1016/j.gca.2013.10.025>.
- [141] R. Mathew, B. Stevenson, A. Tilocca, M. Edén, Toward a rational design of bioactive glasses with optimal structural features: composition–structure correlations unveiled by solid-state NMR and MD simulations, *J. Phys. Chem. B* 118 (2014) 833–844, <https://doi.org/10.1021/jp409652k>.
- [142] N. Stone-Weiss, H. Bradtmüller, M. Fortino, M. Bertani, R.E. Youngman, A. Pedone, H. Eckert, A. Goel, Combined experimental and computational approach toward the structural design of borosilicate-based bioactive glasses, *J. Phys. Chem. C* 124 (2020) 17655–17674, <https://doi.org/10.1021/acs.jpcc.0c04470>.
- [143] C. Massobrio, J. Du, M. Bernasconi, P.S. Salmon (Eds.), *Molecular Dynamics Simulations of Disordered Materials: From Network Glasses to Phase-Change Memory Alloys*, Springer International Publishing, 2015, <https://doi.org/10.1007/978-3-319-15675-0>.

- [144] K.T. Tang, J.P. Toennies, An improved simple model for the van der Waals potential based on universal damping functions for the dispersion coefficients, *J. Chem. Phys.* 80 (1984) 3726–3741, <https://doi.org/10.1063/1.447150>.
- [145] A.J. Stone, Intermolecular forces, in: A.J. Barnes, W.J. Orville-Thomas, J. Yarwood (Eds.), *Mol. Liq. Dyn. Interact.*, Springer Netherlands, Dordrecht, 1984, pp. 1–34, https://doi.org/10.1007/978-94-009-6463-1_1.
- [146] A. Aguado, L. Bernasconi, P.A. Madden, Interionic potentials from *ab initio* molecular dynamics: The alkaline earth oxides CaO, SrO, and BaO, *J. Chem. Phys.* 118 (2003) 5704–5717, <https://doi.org/10.1063/1.1556074>.
- [147] A. Aguado, L. Bernasconi, S. Jahn, P.A. Madden, Multipoles and interaction potentials in ionic materials from plane-wave-DFT calculations, *Faraday Discuss.* 124 (2003) 171–184, <https://doi.org/10.1039/B30319C>.
- [148] M. Salanne, B. Rotenberg, S. Jahn, R. Vuilleumier, C. Simon, P.A. Madden, Including many-body effects in models for ionic liquids, *Theor. Chem. Accounts* 131 (2012) 1143, <https://doi.org/10.1007/s00214-012-1143-9>.
- [149] F. Pacaud, J.-M. Delaye, T. Charpentier, L. Cormier, M. Salanne, Structural study of Na₂O–B₂O₃–SiO₂ glasses from molecular simulations using a polarizable force field, *J. Chem. Phys.* 147 (2017), 161711, <https://doi.org/10.1063/1.4992799>.
- [150] M.F. Guest, A.M. Elena, A.B.G. Chalk, DL_POLY - A performance overview analysing, understanding and exploiting available HPC technology, *Mol. Simul.* 47 (2021) 194–227, <https://doi.org/10.1080/08927022.2019.1603380>.
- [151] A.P. Thompson, H.M. Aktulga, R. Berger, D.S. Bolintineanu, W.M. Brown, P. S. Crozier, P.J. in't Veld, A. Kohlmeier, S.G. Moore, T.D. Nguyen, R. Shan, M. Stevens, J. Tranchida, C. Trott, S.J. Plimpton, LAMMPS - a flexible simulation tool for particle-based materials modeling at the atomic, meso, and continuum scales, *Comput. Phys. Commun.* 271 (2022), 108171, <https://doi.org/10.1016/j.cpc.2021.108171>.
- [152] S. Paramore, L. Cheng, B.J. Berne, A systematic comparison of pairwise and many-body silica potentials, *J. Chem. Theory Comput.* 4 (2008) 1698–1708, <https://doi.org/10.1021/ct800244q>.
- [153] D. Marrocchelli, M. Salanne, P.A. Madden, C. Simon, P. Turq, The construction of a reliable potential for GeO₂ from first principles, *Mol. Phys.* 107 (2009) 443–452, <https://doi.org/10.1080/00268970902845347>.
- [154] J.K. Maranas, Y. Chen, D.K. Stillinger, F.H. Stillinger, Polarization interactions and boroxol ring formation in boron oxide: A molecular dynamics study, *J. Chem. Phys.* 115 (2001) 6578–6589, <https://doi.org/10.1063/1.1401817>.
- [155] J. Tersoff, New empirical model for the structural properties of silicon, *Phys. Rev. Lett.* 56 (1986) 632–635, <https://doi.org/10.1103/PhysRevLett.56.632>.
- [156] J. Tersoff, New empirical-approach for the structure and energy of covalent systems, *Phys. Rev. B* 37 (1988) 6991–7000, <https://doi.org/10.1103/PhysRevB.37.6991>.
- [157] L. Huang, J. Kieffer, Thermomechanical anomalies and polyamorphism in B2O₃ glass: A molecular dynamics simulation study, *Phys. Rev. B* 74 (2006), 224107, <https://doi.org/10.1103/PhysRevB.74.224107>.
- [158] L. Huang, J. Kieffer, Structural origin of negative thermal expansion in high-temperature silica polymorphs, *Phys. Rev. Lett.* 95 (2005), 215901, <https://doi.org/10.1103/PhysRevLett.95.215901>.
- [159] L. Huang, M. Durandurdı, J. Kieffer, Transformation pathways of silica under high pressure, *Nat. Mater.* 5 (2006) 977–981, <https://doi.org/10.1038/nmat1760>.
- [160] S.H. Garofalini, Molecular dynamics computer simulations of silica surface structure and adsorption of water molecules, *J. Non-Cryst. Solids* 120 (1990) 1–12, [https://doi.org/10.1016/0022-3093\(90\)90184-N](https://doi.org/10.1016/0022-3093(90)90184-N).
- [161] B.P. Feuston, S.H. Garofalini, Water-induced relaxation of the vitreous silica surface, *J. Appl. Phys.* 68 (1990) 4830–4836, <https://doi.org/10.1063/1.346142>.
- [162] T.S. Mahadevan, S.H. Garofalini, Dissociative water potential for molecular dynamics simulations, *J. Phys. Chem. B* 111 (2007) 8919–8927, <https://doi.org/10.1021/jp072530o>.
- [163] T.S. Mahadevan, S.H. Garofalini, Dissociative chemisorption of water onto silica surfaces and formation of hydronium ions, *J. Phys. Chem. C* 112 (2008) 1507–1515, <https://doi.org/10.1021/jp076936c>.
- [164] G.K. Lockwood, S.H. Garofalini, Proton dynamics at the water–silica interface via dissociative molecular dynamics, *J. Phys. Chem. C* 118 (2014) 29750–29759, <https://doi.org/10.1021/jp507640y>.
- [165] M. Kagan, G.K. Lockwood, S.H. Garofalini, Reactive simulations of the activation barrier to dissolution of amorphous silica in water, *Phys. Chem. Chem. Phys.* 16 (2014) 9294–9301, <https://doi.org/10.1039/C4CP00030G>.
- [166] A.C.T. van Duin, S. Dasgupta, F. Lorant, W.A. Goddard III, ReaxFF: A reactive force field for hydrocarbons, *J. Phys. Chem. A* 105 (2001) 9396–9409.
- [167] J.M. Rimsza, J. Du, Interfacial structure and evolution of the water–silica gel system by reactive force-field-based molecular dynamics simulations, *J. Phys. Chem. C* 121 (2017) 11534–11543, <https://doi.org/10.1021/acs.jpcc.7b02734>.
- [168] J.M. Rimsza, J. Du, Nanoporous silica gel structures and evolution from reactive force field-based molecular dynamics simulations, *Npj Mater. Degrad.* 2 (2018) 18, <https://doi.org/10.1038/s41529-018-0039-o>.
- [169] T.P. Senftle, S. Hong, M.M. Islam, S.B. Kylasa, Y. Zheng, Y.K. Shin, C. Junkermeier, R. Engel-Herbert, M.J. Janik, H.M. Aktulga, others, The ReaxFF reactive force-field: development, applications and future directions, *Npj Comput. Mater.* 2 (2016) 15011, <https://doi.org/10.1038/npjcomputats.2015.11>.
- [170] A.K. Rappe, W.A. Goddard, Charge equilibration for molecular dynamics simulations, *J. Phys. Chem.* 95 (1991) 3358–3363, <https://doi.org/10.1021/j100161a070>.
- [171] A.C.T. van Duin, A. Strachan, S. Stewman, Q. Zhang, X. Xu, W.A. Goddard, ReaxFF/SiO reactive force field for silicon and silicon oxide systems, *J. Phys. Chem. A* 107 (2003) 3803–3811, <https://doi.org/10.1021/jp0276303>.
- [172] Y. Yu, B. Wang, M. Wang, G. Sant, M. Bauchy, Revisiting silica with ReaxFF: Towards improved predictions of glass structure and properties via reactive molecular dynamics, *J. Non-Cryst. Solids* 443 (2016) 148–154, <https://doi.org/10.1016/j.jnoncrysol.2016.03.026>.
- [173] J.C. Fogarty, H.M. Aktulga, A.Y. Grama, A.C.T. van Duin, S.A. Pandit, A reactive molecular dynamics simulation of the silica–water interface, *J. Chem. Phys.* 132 (2010), 174704, <https://doi.org/10.1063/1.3407433>.
- [174] J. Yeon, A.C.T. van Duin, ReaxFF molecular dynamics simulations of hydroxylation kinetics for amorphous and nano-silica structure, and its relations with atomic strain energy, *J. Phys. Chem. C* 120 (2016) 305–317, <https://doi.org/10.1021/acs.jpcc.5b09784>.
- [175] J.M. Rimsza, J. Yeon, A.C.T. van Duin, J. Du, Water interactions with nanoporous silica: comparison of ReaxFF and ab initio based molecular dynamics simulations, *J. Phys. Chem. C* 120 (2016) 24803–24816, <https://doi.org/10.1021/acs.jpcc.6b07939>.
- [176] A. Macià Escalart, P. Ugliengo, S.T. Bromley, Modeling hydroxylated nanosilica: Testing the performance of ReaxFF and FFSSiOH force fields, *J. Chem. Phys.* 146 (2017), 224704, <https://doi.org/10.1063/1.4985083>.
- [177] T.S. Mahadevan, J. Du, Evaluating water reactivity at silica surfaces using reactive potentials, *J. Phys. Chem. C* 122 (2018) 9875–9885, <https://doi.org/10.1021/acs.jpcc.7b12653>.
- [178] W. Zhang, A.C.T. van Duin, Second-Generation ReaxFF water force field: improvements in the description of water density and OH-Anion diffusion, *J. Phys. Chem. B* 121 (2017) 6021–6032, <https://doi.org/10.1021/acs.jpbc.7b02548>.
- [179] T.S. Mahadevan, W. Sun, J. Du, Development of water reactive potentials for sodium silicate glasses, *J. Phys. Chem. B* 123 (2019) 4452–4461, <https://doi.org/10.1021/acs.jpcb.9b02216>.
- [180] T.S. Mahadevan, J. Du, Hydration and reaction mechanisms on sodium silicate glass surfaces from molecular dynamics simulations with reactive force fields, *J. Am. Ceram. Soc.* 103 (2020) 3676–3690, <https://doi.org/10.1111/jace.17059>.
- [181] T.S. Mahadevan, J. Du, Atomic and micro-structure features of nanoporous aluminosilicate glasses from reactive molecular dynamics simulations, *J. Am. Ceram. Soc.* 104 (2021) 229–242, <https://doi.org/10.1111/jace.17465>.
- [182] Y. Yu, B. Wang, M. Wang, G. Sant, M. Bauchy, Reactive molecular dynamics simulations of sodium silicate glasses — toward an improved understanding of the structure, *Int. J. Appl. Glas. Sci.* 8 (2017) 276–284, <https://doi.org/10.1111/jag.12248>.
- [183] S.H. Hahn, J. Rimsza, L. Criscenti, W. Sun, L. Deng, J. Du, T. Liang, S.B. Sinnott, A.C.T. van Duin, Development of a ReaxFF reactive force field for NaSiO_x/water systems and its application to sodium and proton self-diffusion, *J. Phys. Chem. C* 122 (2018) 19613–19624, <https://doi.org/10.1021/acs.jpcc.8b05582>.
- [184] R. Dongol, L. Wang, A.N. Cormack, S.K. Sundaram, Molecular dynamics simulation of sodium aluminosilicate glass structures and glass surface–water reactions using the reactive force field (ReaxFF), *Appl. Surf. Sci.* 439 (2018) 1103–1110, <https://doi.org/10.1016/j.apsusc.2017.12.180>.
- [185] J. Yeon, S.C. Chowdhury, C.M. Daksha, J.W. Gillespie, Development of Mg/Al/Si/O ReaxFF parameters for magnesium aluminosilicate glass using an artificial neural network-assisted genetic algorithm, *J. Phys. Chem. C* 125 (2021) 18380–18394, <https://doi.org/10.1021/acs.jpcc.1c01190>.
- [186] L. Deng, K. Miyatani, S. Amma, M. Suehara, M. Ono, Y. Yamamoto, S. Urata, J. Du, Reaction mechanisms and interfacial behaviors of sodium silicate glass in an aqueous environment from reactive force field-based molecular dynamics simulations, *J. Phys. Chem. C* 123 (2019) 21538–21547, <https://doi.org/10.1021/acs.jpcc.9b05030>.
- [187] S.H. Hahn, A.C.T. van Duin, Surface reactivity and leaching of a sodium silicate glass under an aqueous environment: A ReaxFF molecular dynamics study, *J. Phys. Chem. C* 123 (2019) 15606–15617, <https://doi.org/10.1021/acs.jpcc.9b02940>.
- [188] H. Jabraoui, S. Gin, T. Charpentier, R. Pollet, J.-M. Delaye, Leaching and reactivity at the sodium aluminosilicate glass–water interface: insights from a ReaxFF molecular dynamics study, *J. Phys. Chem. C* 125 (2021) 27170–27184, <https://doi.org/10.1021/acs.jpcc.1c07266>.
- [189] J.M. Rimsza, R.E. Jones, L.J. Criscenti, Surface structure and stability of partially hydroxylated silica surfaces, *Langmuir* 33 (2017) 3882–3891, <https://doi.org/10.1021/acs.langmuir.7b00041>.
- [190] J.M. Rimsza, R.E. Jones, L.J. Criscenti, Mechanisms of silica fracture in aqueous electrolyte solutions, *Front. Mater.* 6 (2019), <https://doi.org/10.3389/fmats.2019.00079>.
- [191] J.M. Rimsza, R.E. Jones, L.J. Criscenti, Chemical effects on subcritical fracture in silica from molecular dynamics simulations, *J. Geophys. Res. Solid Earth* 123 (2018) 9341–9354, <https://doi.org/10.1029/2018JB016120>.
- [192] J. Wen, T. Ma, W. Zhang, A.C.T. van Duin, X. Lu, Atomistic mechanisms of Si chemical mechanical polishing in aqueous H₂O₂: ReaxFF reactive molecular dynamics simulations, *Comput. Mater. Sci.* 131 (2017) 230–238, <https://doi.org/10.1016/j.commatsci.2017.02.005>.
- [193] J. Wen, T. Ma, W. Zhang, G. Psolfogiannakis, A.C.T. van Duin, L. Chen, L. Qian, Y. Hu, X. Lu, Atomic insight into tribocorrosion mechanism of silicon at the Si/SiO_x interface in aqueous environment: Molecular dynamics simulations using ReaxFF reactive force field, *Appl. Surf. Sci.* 390 (2016) 216–223, <https://doi.org/10.1016/j.apsusc.2016.08.082>.
- [194] X. Guo, S. Yuan, J. Huang, C. Chen, R. Kang, Z. Jin, D. Guo, Effects of pressure and slurry on removal mechanism during the chemical mechanical polishing of quartz glass using ReaxFF MD, *Appl. Surf. Sci.* 505 (2020), 144610, <https://doi.org/10.1016/j.apsusc.2019.144610>.

- [195] X. Guo, J. Huang, S. Yuan, R. Kang, D. Guo, Study using ReaxFF-MD on the CMP process of fused glass in pure H₂O/aqueous H₂O₂, *Appl. Surf. Sci.* (2021), 149756, <https://doi.org/10.1016/j.apsusc.2021.149756>.
- [196] L. Deng, S. Urata, Y. Takimoto, T. Miyajima, S.H. Hahn, A.C.T. van Duin, J. Du, Structural features of sodium silicate glasses from reactive force field-based molecular dynamics simulations, *J. Am. Ceram. Soc.* 103 (2020) 1600–1614, <https://doi.org/10.1111/jace.16837>.
- [197] A.K. Rappe, W.A. Goddard III, Charge equilibration for molecular dynamics simulations, *J. Phys. Chem.* 95 (1991) 3358–3363, <https://doi.org/10.1021/j100161a070>.
- [198] Y. Han, D. Jiang, J. Zhang, W. Li, Z. Gan, J. Gu, Development, applications and challenges of ReaxFF reactive force field in molecular simulations, *Front. Chem. Sci. Eng.* 10 (2016) 16–38, <https://doi.org/10.1007/s11705-015-1545-z>.
- [199] L. Liu, Y. Liu, S.V. Zybin, H. Sun, W.A. Goddard, ReaxFF-Ig: Correction of the ReaxFF reactive force field for London dispersion, with applications to the equations of state for energetic materials, *J. Phys. Chem. A* 115 (2011) 11016–11022, <https://doi.org/10.1021/jp201599t>.
- [200] J.D. Gale, Empirical potential derivation for ionic materials, *Philos. Mag. B* 73 (1996) 3–19, <https://doi.org/10.1080/13642819608239107>.
- [201] R.D. Oeffner, S.R. Elliott, Interatomic potential for germanium dioxide empirically fitted to an ab initio energy surface, *Phys. Rev. B* 58 (1998) 14791–14803, <https://doi.org/10.1103/PhysRevB.58.14791>.
- [202] A.C. Lasaga, G.V. Gibbs, Applications of quantum mechanical potential surfaces to mineral physics calculations, *Phys. Chem. Miner.* 14 (1987) 107–117, <https://doi.org/10.1007/BF00308214>.
- [203] A. Pedone, M. Corno, B. Civalleri, G. Malavasi, M.C. Menziani, U. Segre, P. Ugliengo, An ab initio parameterized interatomic force field for hydroxyapatite, *J. Mater. Chem.* 17 (2007) 2061–2068, <https://doi.org/10.1039/b61785h>.
- [204] R. Car, M. Parrinello, Unified approach for molecular dynamics and density-functional theory, *Phys. Rev. Lett.* 55 (1985) 2471–2474, <https://doi.org/10.1103/PhysRevLett.55.2471>.
- [205] K. Konstantinou, P.V. Sushko, D.M. Duffy, Modelling the local atomic structure of molybdenum in nuclear waste glasses with ab initio molecular dynamics simulations, *Phys. Chem. Chem. Phys.* 18 (2016) 26125–26132, <https://doi.org/10.1039/C6CP03076A>.
- [206] A. Carré, J. Horbach, S. Ispas, W. Kob, New fitting scheme to obtain effective potential from Car-Parrinello molecular-dynamics simulations: Application to silica, *EPL Europhys. Lett.* 82 (2008) 17001, <https://doi.org/10.1209/0295-5075/82/17001>.
- [207] R. Fletcher, *Practical Methods of Optimization*, 2nd edition, Wiley, Chichester; New York, 1987.
- [208] J.J. Moré, The Levenberg-Marquardt algorithm: implementation and theory, in: G.A. Watson (Ed.), *Numer. Anal.*, Springer, Berlin, Heidelberg, 1978, pp. 105–116, <https://doi.org/10.1007/BFb0067700>.
- [209] E. Brochu, V.M. Cora, N. de Freitas, A Tutorial on Bayesian Optimization of Expensive Cost Functions, with Application to Active User Modeling and Hierarchical Reinforcement Learning, *ArXiv10122599 Cs*, 2010, <https://doi.org/10.48550/arXiv.1012.2599>.
- [210] P.I. Frazier, J. Wang, Bayesian optimization for materials design, in: T. Lookman, F.J. Alexander, K. Rajan (Eds.), *Inf. Sci. Mater. Discov. Des.*, Springer International Publishing, Cham, 2016, pp. 45–75, https://doi.org/10.1007/978-3-319-23871-5_3.
- [211] C.E. Rasmussen, C.K.I. Williams, *Gaussian Processes for Machine Learning*, MIT Press, Cambridge, MA, USA, 2005.
- [212] H. Liu, Z. Fu, Y. Li, N.F.A. Sabri, M. Bauchy, Parameterization of empirical forcefields for glassy silica using machine learning, *MRS Commun.* 9 (2019) 593–599, <https://doi.org/10.1557/mrc.2019.47>.
- [213] S. Urata, T. Miyajima, N. Kayaba, L. Deng, J. Du, Development of a force field for modeling lithium borosilicate glasses, *Int. J. Appl. Glas. Sci.* 13 (2022) 444–456, <https://doi.org/10.1111/jag.16570>.
- [214] R. Christensen, S.S. Sørensen, H. Liu, K. Li, M. Bauchy, M.M. Smetskjaer, Interatomic potential parameterization using particle swarm optimization: Case study of glassy silica, *J. Chem. Phys.* 154 (2021), 134505, <https://doi.org/10.1063/5.0041183>.
- [215] D. Wang, D. Tan, L. Liu, Particle swarm optimization algorithm: an overview, *Soft. Comput.* 22 (2018) 387–408, <https://doi.org/10.1007/s00500-016-2474-6>.
- [216] M. Kumar, D.M. Husain, N. Upreti, D. Gupta, Genetic algorithm: review and application, *Soc. Sci. Res. Netw. Rochester NY* (2010), <https://doi.org/10.2139/ssrn.3529843>.
- [217] W.S. McCulloch, W. Pitts, A logical calculus of the ideas immanent in nervous activity, *Bull. Math. Biol.* 52 (1990) (1943) 99–115 (discussion 73–97).
- [218] J. Zupan, J. Gasteiger, Neural Networks for Chemists. An Introduction, VCH Pub, Weinheim, 1993, <https://doi.org/10.1002/cem.1180080410>.
- [219] J. Behler, Four generations of high-dimensional neural network potentials, *Chem. Rev.* 121 (2021) 10037–10072, <https://doi.org/10.1021/acs.chemrev.0c00868>.
- [220] V. Botu, R. Batra, J. Chapman, R. Ramprasad, Machine learning force fields: construction, validation, and outlook, *J. Phys. Chem. C* 121 (2017) 511–522, <https://doi.org/10.1021/acs.jpcc.6b10908>.
- [221] O.T. Unke, S. Chmiela, H.E. Sauceda, M. Gastegger, I. Poltavsky, K.T. Schütt, A. Tkatchenko, K.-R. Müller, Machine learning force fields, *Chem. Rev.* 121 (2021) 10142–10186, <https://doi.org/10.1021/acs.chemrev.0c01111>.
- [222] H. Wang, L. Zhang, J. Han, W. E, DeePMD-kit: A deep learning package for many-body potential energy representation and molecular dynamics, *Comput. Phys. Commun.* 228 (2018) 178–184, <https://doi.org/10.1016/j.cpc.2018.03.016>.
- [223] L. Zhang, J. Han, H. Wang, R. Car, W. E, Deep potential molecular dynamics: a scalable model with the accuracy of quantum mechanics, *Phys. Rev. Lett.* 120 (2018), 143001, <https://doi.org/10.1103/PhysRevLett.120.143001>.
- [224] T. Wen, L. Zhang, H. Wang, W. E, D.J. Srolovitz, Deep potentials for materials science, *Mater. Futur.* 1 (2022), 022601, <https://doi.org/10.1088/2752-5724/ac681d>.
- [225] L. Zhang, J. Han, H. Wang, W. Saidi, R. Car, W. E, End-to-end symmetry preserving inter-atomic potential energy model for finite and extended systems, in: *Adv. Neural Inf. Process. Syst.*, Curran Associates, Inc 31, 2018.
- [226] J. Behler, M. Parrinello, Generalized neural-network representation of high-dimensional potential-energy surfaces, *Phys. Rev. Lett.* 98 (2007), 146401, <https://doi.org/10.1103/PhysRevLett.98.146401>.
- [227] J. Behler, Atom-centered symmetry functions for constructing high-dimensional neural network potentials, *J. Chem. Phys.* 134 (2011), 074106, <https://doi.org/10.1063/1.3553717>.
- [228] A.P. Bartók, J. Kermode, N. Bernstein, G. Csányi, Machine learning a general-purpose interatomic potential for silicon, *Phys. Rev. X* 8 (2018), 041048, <https://doi.org/10.1103/PhysRevX.8.041048>.
- [229] A.P. Bartók, R. Kondor, G. Csányi, On representing chemical environments, *Phys. Rev. B* 87 (2013), 184115, <https://doi.org/10.1103/PhysRevB.87.184115>.
- [230] Y. Zhang, H. Wang, W. Chen, J. Zeng, L. Zhang, H. Wang, W. E, DP-GEN: A concurrent learning platform for the generation of reliable deep learning based potential energy models, *Comput. Phys. Commun.* 253 (2020), 107206, <https://doi.org/10.1016/j.cpc.2020.107206>.
- [231] A.P. Bartók, M.C. Payne, R. Kondor, G. Csányi, Gaussian approximation potentials: the accuracy of quantum mechanics, without the electrons, *Phys. Rev. Lett.* 104 (2010), 136403, <https://doi.org/10.1103/PhysRevLett.104.136403>.
- [232] M. Rupp, A. Tkatchenko, K.-R. Müller, O.A. von Lilienfeld, Fast and accurate modeling of molecular atomization energies with machine learning, *Phys. Rev. Lett.* 108 (2012), 058301, <https://doi.org/10.1103/PhysRevLett.108.058301>.
- [233] T.W. Ko, J.A. Finkler, S. Goedecker, J. Behler, A fourth-generation high-dimensional neural network potential with accurate electrostatics including non-local charge transfer, *Nat. Commun.* 12 (2021) 398, <https://doi.org/10.1038/s41467-020-20427-2>.
- [234] N. Artrith, T. Morawietz, J. Behler, High-dimensional neural-network potentials for multicomponent systems: Applications to zinc oxide, *Phys. Rev. B* 83 (2011), 153101, <https://doi.org/10.1103/PhysRevB.83.153101>.
- [235] A. Grisafi, M. Cerotti, Incorporating long-range physics in atomic-scale machine learning, *J. Chem. Phys.* 151 (2019), 204105, <https://doi.org/10.1063/1.5128375>.
- [236] O.T. Unke, M. Meuwly, PhysNet: A neural network for predicting energies, forces, dipole moments, and partial charges, *J. Chem. Theory Comput.* 15 (2019) 3678–3693, <https://doi.org/10.1021/acs.jctc.9b00181>.
- [237] S.A. Ghasemi, A. Hoffstetter, S. Saha, S. Goedecker, Interatomic potentials for ionic systems with density functional accuracy based on charge densities obtained by a neural network, *Phys. Rev. B* 92 (2015), 045131, <https://doi.org/10.1103/PhysRevB.92.045131>.
- [238] R. Jinnochi, J. Lahnsteiner, F. Karsai, G. Kresse, M. Bokdam, Phase transitions of hybrid perovskites simulated by machine-learning force fields trained on the fly with Bayesian inference, *Phys. Rev. Lett.* 122 (2019), 225701, <https://doi.org/10.1103/PhysRevLett.122.225701>.
- [239] M. Gastegger, L. Schwiedrzik, M. Bittermann, F. Berzenyi, P. Marquetand, wACSF—Weighted atom-centered symmetry functions as descriptors in machine learning potentials, *J. Chem. Phys.* 148 (2018), 241709, <https://doi.org/10.1063/1.5019667>.
- [240] K. Schütt, P.-J. Kindermans, H.E. Sauceda Felix, S. Chmiela, A. Tkatchenko, K.-R. Müller, SchNet: A continuous-filter convolutional neural network for modeling quantum interactions, *Adv. Neural Inf. Process. Syst. Curr. Assoc. Inc.* (2017) 992–1002, in: <https://proceedings.neurips.cc/paper/2017/file/303ed4c69846ab36c2904d3ba8573050-Paper.pdf>.
- [241] C.W. Park, M. Kornbluth, J. Vandermause, C. Wolverton, B. Kozinsky, J.P. Mailoa, Accurate and scalable graph neural network force field and molecular dynamics with direct force architecture, *Npj Comput. Mater.* 7 (2021) 1–9, <https://doi.org/10.1038/s41524-021-00543-3>.
- [242] S. Batzner, A. Musaelian, L. Sun, M. Geiger, J.P. Mailoa, M. Kornbluth, N. Molinari, T.E. Smidt, B. Kozinsky, E(3)-equivariant graph neural networks for data-efficient and accurate interatomic potentials, *Nat. Commun.* 13 (2022) 2453, <https://doi.org/10.1038/s41467-022-29939-5>.
- [243] Z. Li, K. Meidani, P. Yadav, A. Barati Farimani, Graph neural networks accelerated molecular dynamics, *J. Chem. Phys.* 156 (2022), 144103, <https://doi.org/10.1063/5.0083060>.
- [244] X. Wang, Y. Xu, H. Zheng, K. Yu, A scalable graph neural network method for developing an accurate force field of large flexible organic molecules, *J. Phys. Chem. Lett.* 12 (2021) 7982–7987, <https://doi.org/10.1021/acs.jpclett.1c02214>.
- [245] I.A. Balyakin, S.V. Rempel, R.E. Ryltsev, A.A. Rempel, Deep machine learning interatomic potential for liquid silica, *Phys. Rev. E* 102 (2020), 052125, <https://doi.org/10.1103/PhysRevE.102.052125>.
- [246] G. Bebis, M. Georgopoulos, Feed-forward neural networks, *IEEE Potentials.* 13 (1994) 27–31, <https://doi.org/10.1109/45.329294>.
- [247] S. Urata, N. Nakamura, T. Tada, A.R. Tan, R. Gómez-Bombarelli, H. Hosono, Suppression of Rayleigh Scattering in silica glass by codoping boron and fluorine: molecular dynamics simulations with force-matching and neural network potentials, *J. Phys. Chem. C* 126 (2022) 2264–2275, <https://doi.org/10.1021/acs.jpcc.1c10300>.

- [248] L.C. Erhard, J. Rohrer, K. Albe, V.L. Deringer, A machine-learned interatomic potential for silica and its relation to empirical models, *Npj Comput. Mater.* 8 (2022) 1–12, <https://doi.org/10.1038/s41524-022-00768-w>.
- [249] Z. Wu, S. Pan, F. Chen, G. Long, C. Zhang, P.S. Yu, A comprehensive survey on graph neural networks, *IEEE Trans. Neural Netw. Learn. Syst.* 32 (2021) 4–24, <https://doi.org/10.1109/TNNLS.2020.2978386>.
- [250] W. Li, Y. Ando, E. Minamitani, S. Watanabe, Study of Li atom diffusion in amorphous Li₃PO₄ with neural network potential, *J. Chem. Phys.* 147 (2017), 214106, <https://doi.org/10.1063/1.4997242>.
- [251] W. Li, Y. Ando, Comparison of different machine learning models for the prediction of forces in copper and silicon dioxide, *Phys. Chem. Chem. Phys.* 20 (2018) 30006–30020, <https://doi.org/10.1039/C8CP04508A>.
- [252] T.L. Pham, H. Kino, K. Terakura, T. Miyake, H.C. Dam, Novel mixture model for the representation of potential energy surfaces, *J. Chem. Phys.* 145 (2016), 154103, <https://doi.org/10.1063/1.4964318>.
- [253] J.P. Mailoa, M. Kornbluth, S. Batzner, G. Samsonidze, S.T. Lam, J. Vandermause, C. Abllitt, N. Molinari, B. Kozinsky, A fast neural network approach for direct covariant forces prediction in complex multi-element extended systems, *Nat. Mach. Intell.* 1 (2019) 471–479, <https://doi.org/10.1038/s42256-019-0098-0>.